UNIVERSITY OF OKLAHOMA

GRADUATE COLLEGE

STUDY ON SELECT DESIGN FACTORS IN GRS BRIDGE ABUTMENTS

A THESIS

SUBMITTED TO THE GRADUATE FACULTY

in partial fulfillment of the requirements for the

Degree of

MASTER OF SCIENCE

By

SAFAL SHARMA POUDEL
Norman, Oklahoma
2025

STUDY ON SELECT DESIGN FACTORS IN GRS BRIDGE ABUTMENTS

A THESIS APPROVED FOR THE
SCHOOL OF CIVIL ENGINEERING AND ENVIRONMENTAL SCIENCE

BY THE COMMITTEE CONSISTING OF

Dr. Kianoosh Hatami, Chair

Dr. Kanthasamy Muraleetharan

Dr. Hamed Mirzaeifar

Dedication

I want to dedicate this thesis to my parents for their unwavering love, support, and sacrifices. Without them, I wouldn't be where I am today. I also dedicate this work to my siblings, cousins, and friends who have always encouraged and supported me throughout this journey.

Finally, I dedicate this thesis to the Almighty God for giving me strength, guidance, and blessings throughout this journey.

Acknowledgments

I am sincerely grateful to Dr. Kianoosh Hatami for providing me the opportunity to conduct research under his supervision throughout my Master's degree. His constant support and mentorship have helped me grow both academically and professionally. I would also like to thank my committee members, Dr. Hamed Mirzaeifar and Dr. Kanthasamy Muraleetharan, for their constructive feedback and suggestions. I especially thank Dr. Mirzaeifar for supporting me as a mentor even before this research began.

A very special thanks to Dr. Hideto Nonoyama for helping me set up my experiments, guiding me through each step, and giving detailed feedback on my writing. His support has been a valuable component of my research work. I would also like to acknowledge the undergraduate researchers who assisted me in constructing the model abutments, including Jack Anderson and Layne Barton, and all the members of Dr. Hatami's research group for their help throughout this work.

I also would like to acknowledge Dr. Amy Cerato and Dr. Tommy Bounds for their support during the laboratory tests carried out at the Soil Mechanics Laboratory in the School of Civil Engineering and Environmental Science. Additionally, I appreciate Dr. Royce Floyd for helping me to understand the data acquisition system at the beginning of the research and Mr. John Bullock for making my work easier at the Fears Laboratory. Finally, I want to thank all my friends in Norman. Their companionship made my stay here pleasant and valuable.

Table of Contents

List of Tables

List of Figures

Abstract

Construction of Geosynthetic Reinforced Soil (GRS) bridge abutments requires high-quality coarse-grained backfill materials. But the increasing scarcity of select fills has driven up construction costs, creating a demand for more affordable alternatives. To address this economic concern, this study examines the viability of using a marginal quality soil as backfill material for GRS bridge abutments. The marginal soil used in this study had nearly 25% fines, but it was non-plastic. Three model walls with identical designs were constructed: Model 1 with sand backfill (control case) and Models 2 and 3 with the marginal soil as the backfill, which was placed and compacted in both models at OMC+3% gravimetric water content. The strip footing, representing bridge load, was at the same location for Models 1 and 2, but it was placed closer to the abutment facing in Model 3. Each model abutment was instrumented to monitor settlements, facing displacements, reinforcement strains, and water content at selected locations within each model.

Results of the study showed that Model 2 exhibited slightly larger deformation than the control model and Model 3 showed greater deformations than Model 2 due to the proximity of the strip footing load to its facing. Nevertheless, footing settlements, facing displacements and reinforcement strains in all models were significantly smaller than the FHWA serviceability requirements for a 190 kPa design load. These observations indicate that with proper design, including tightly-spaced reinforcement and strong facing-reinforcement connection, as was done in this study, marginal quality backfills of the type used in this study can serve effectively as backfill in GRS bridge abutments. The study provides valuable insight into the influences that backfill quality and footing location could have on structural stability and performance of GRS

bridge abutments, offering a potential path toward cost-effective backfill alternatives for their design.

1. Introduction

Departments of transportation across the United States continuously face maintenance challenges due to landslides and slope failures along highways. The financial cost associated with addressing such problems through repair and maintenance is significant. In Oklahoma, the prevalence of such failures is notably higher in the eastern and central regions, attributed to their elevated topography and suboptimal soil conditions (Hatami et al., 2010a, b, 2012). According to the design guidelines and specifications for bridge abutment structures in North America, the construction and repair of highway slopes and mechanically stabilized earth (MSE) walls typically require large volumes of coarse-grained, free-draining soils to ensure structural stability (Berg et al., 2009). However, coarse-grained soils are scarce in Oklahoma and various other regions of the U.S. As a result, the expense of acquiring and transporting the fill material can become excessively high, depending on the proximity to sources of high-quality soil.

In scenarios where high-quality offsite soils are scarce and transportation costs become a significant concern, using locally available soils for construction emerges as a viable alternative. This approach drastically reduces the need for extensive material transportation, fuel usage, and environmental pollution. However, the soils readily available in Oklahoma for constructing reinforced slopes often fall into the category of marginal quality; the Federal Highway Administration (FHWA, 2009) specify that backfill materials for Mechanically Stabilized Earth (MSE) wall construction should contain less than 15% fines passing the No. 200 sieve (0.075 mm) and a plasticity index (PI) of less than 6%. For Geosynthetic Reinforced Soil (GRS) bridge abutments, the (FHWA, 2018) recommends fines content of less than 12%. In contrast, the National Cooperative Highway Research Program (NCHRP 24-22, 2013) permits up to 30%

fines for MSE wall backfills, provided material properties are well-defined, and controls are implemented to address potential design challenges such as drainage, corrosion, and reinforcement pullout. The National Concrete Masonry Association (NCMA, 2006) allows up to 35% fines and a PI of up to 20% for MSE wall backfills. Based on the above survey, soils with fine contents between 12% and 35% can be considered as marginal soils.

In this study, the structural benefit of tightly-spaced reinforcement is utilized to investigate the possibility of using marginal soils in GRS bridge abutments to reduce their construction costs. However, the behavior of marginal soils, coupled with their interaction with geosynthetic reinforcements, can present complexities under both construction and operational conditions. These include the potential for the soils to exhibit strain softening, undergo substantial deformation, or experience a reduction in strength due to moisture exposure (Esmaili et al., 2014).

In particular, the potential reduction in interface shear strength or pullout resistance caused by increased moisture content may lead to excessive deformation or even failure. Therefore, any design approach must account for moisture-sensitive behavior and include safety margins to address these concerns. While there is growing interest in using marginal soils for reinforced soil structures, current design methodologies do not provide specific guidelines for GRS abutments with marginal soil backfills.

This study aims to evaluate the feasibility of using marginal soils in GRS bridge abutments by investigating the mechanical performance of model GRS abutments constructed with such soils and comparing them to a control model using select backfill materials. The objective is not to replace existing design guidelines but to supplement them by identifying critical design parameters and quality control measures essential for the effective and reliable use of marginal soils in reinforced soil structures.

2. Literature Review

A review of related literature is provided in this chapter section.

2.1 Pullout Tests and Bearing Capacity of Reinforced Foundations

Lee et al. (1999) performed a series of numerical and model experiments on the performance of a footing laid on a granular fill layer overlying soft clay. The research work focused on the effects of geotextile reinforcement and thickness of the granular fill layer on the ultimate bearing capacity and settlement behavior of the footing. Their results showed that the bearing capacity increased and the settlement decreased significantly with the use of a geotextile reinforcement. At the same time, the optimal thickness of the sand layer was 0.8 times the width of the footing. Their study also showed that geotextile reinforcement reduced the required fill thickness compared to unreinforced systems.

Abu-Farsakh et al. (2006) conducted a study to compare field and laboratory pullout tests of geosynthetic reinforcements in marginal silty clay soil to evaluate soil-geosynthetic interface parameters. Their result highlighted that marginal silty clay as a backfill offered adequate pullout resistance compared to granular backfill. It was observed that weak geogrids exhibited higher strain and normalized shear values compared to stronger ones. Field and laboratory results showed consistency, though variations were attributed to differences in compaction and potential geosynthetic arching.

Kumar et al. (2007) conducted a series of model tests to investigate the bearing capacity of strip footings resting on stratified subsoil composed of a strong sand layer over a weak sand deposit. They observed that reinforcing the top layer, after replacing weak soil with well-graded sand, increased the bearing capacity of the footing up to 3 to 4 times. Their study concluded that multiple layers of reinforcement can enhance stability and reduce settlement in the stratified soil.

Yoo et al. (2007) investigated the pullout and drainage properties of three types of geosynthetics (i.e., geogrid, geotextile, and composite) reinforcement in weathered granite backfill soils with high fine content (25.8~32.9%) and low permeability. Their results from pullout tests and the analysis using the finite difference method (FDM) showed that composite reinforcement with drainage properties (combination of geotextile and geogrid) increased wall stability.

Shivashankar and Jayaraj (2013) conducted a series of laboratory bearing capacity tests to examine the influence of reinforcement on strength enhancement and settlement reduction in granular beds overlying weak soil. Their findings indicated that bearing capacity improvement was influenced by the thickness of the granular bed, the magnitude and direction of prestressing, and the number of reinforcement layers. For a granular bed thickness of B (where B is the width of the footing) with a single layer of uniaxially prestressed reinforcement, the bearing capacity ratio (BCR) increased until the prestress reached 2%, after which it declined. In contrast, biaxial prestressing achieved the maximum BCR at 1% prestress. For a bed thickness of 2B, BCR continued to increase with higher prestress levels in both biaxial and uniaxial conditions. When two reinforcement layers were used, the highest BCR was observed at a prestress of 2% for the bed thickness of B and 3% for the thickness of 2B.

Esmaili et al. (2014) performed multi-scale pullout and interface shear tests to study the influence of soil matric suction on the interface strength between geotextile reinforcement and marginal soil. They developed the Moisture Reduction Factor (MRF) to predict the reduction of pullout resistance due to changes in gravimetric water content. Their results showed that the loss of matric suction resulted in a pullout resistance reduction of up to 42%, highlighting the effect of moisture fluctuation on geotextile-soil interaction. Their results also showed that wetting the soil-geotextile interface during the construction or service life of a reinforced soil structure could measurably reduce the geotextile reinforcement's interface strength and pullout resistance.

Abdi and Mirzaeifar (2017) investigated the effects of grain size and distribution on soil geogrid interactions during pullout tests using three different granular soils reinforced with HDPE geogrid through the combination of pullout tests, particle image velocimetry (PIV), and finite element analysis (FEA). Their study indicated that larger grain sizes increase pullout forces and thicker shear zones, with particles near geogrid ribs displaying circular displacement patterns. Their results also highlighted that coarser, non-uniform soils show greater pullout resistance due to better particle interlocking and soil-geogrid interactions, also verified by FEA.

Mirzaalimohammadi et al. (2019) investigated the pullout behavior of geosynthetics reinforced with added components: Geogrid-Bar (GGB) and Geocomposite-Pin (GCP). Their findings revealed that these systems significantly enhanced pullout resistance, with GGB and GCP increasing resistance by 37% and 46%, respectively, compared to conventional geosynthetics. Their findings also demonstrated that optimizing the placement and number of reinforcing elements could further increase reinforcement efficiency.

Mirzaeifar et al. (2022) conducted a comprehensive experimental study to evaluate the pullout behavior of uniaxial geogrids embedded in fine-grained soils with and without thin granular drainage layers using PIV. The study explored the effects of gravimetric water content (5–20%), overburden pressure (25–100 kPa), and layer thickness (50 mm and 100 mm of sand or gravel) on geogrid pullout resistance. Results showed that encapsulating geogrids within granular layers significantly enhanced pullout resistance, especially under higher confining pressures and wetter conditions. PIV results revealed that thicker and coarser granular layers expanded the shear zone, enhancing soil-geogrid interaction. The findings suggest that such reinforcement-drainage systems can enhance the performance of MSE walls constructed with marginal soil, particularly under unsaturated and variable moisture conditions.

2.2 MSE Walls with Marginal Soil Backfills

Sandri (2005) discussed the challenges and considerations in constructing MSE walls with marginal fills. The author highlighted potential risks associated with using marginal soils, such as pore water pressure generation, seepage issues, and reduced shear strength due to wetting. These risks could be mitigated by providing special drainage measures, which include the use of geosynthetic materials, drainage composites, and proper surface runoff management.

Bilgin and Kim (2010) studied the effect of reinforcement length and soil properties on the deformation behavior of MSE walls using finite element analysis. Their result indicated that the reduction in reinforcement length from 0.7 times the wall height (0.7H) to 0.4H could increase the wall deformation by more than 80% and reinforcement load by up to 20%. Their results also indicated that an increase in soil friction angle from 30^o to 42^o could reduce the maximum wall deformation by up to 50%.

Hatami et al. (2012) investigated the influence of backfill moisture content on the pullout capacity of geotextile reinforcement in MSE walls using marginal soils. The research highlighted that an increase in moisture content reduces the matric suction, significantly reducing the pullout capacity of the geotextile and the soil-reinforcement interface shear strength. The large-scale pullout tests demonstrated a 37% reduction in pullout capacity when the soil was compacted at moisture levels 2% higher than the optimum. In comparison, small-scale tests indicated a reduction of about 47%. Their study introduced Moisture Reduction Factors (MRFs) to quantify these reductions.

Yoo (2013) conducted a numerical investigation with a finite element model to study the performance of geosynthetic reinforced soil walls under rainfall conditions. The results indicated significant increases in displacement and reinforcement loads for walls backfilled with marginal soils, leading to slope instability. At the end of construction, further displacement in the wall continued up to 90 mm at the elevation of one-third of the total wall height from the base. It was also observed that the reinforcement load increased during rainfall due to the wall displacement.

Riccio et al. (2014) studied the performance of a block-faced geogrid-reinforced wall constructed with fine-grained soil as backfill. They found that the unsaturated conditions of the fine-grained soil led to significant apparent cohesion due to soil suction, which influenced the wall's stability. Soil compaction impacted reinforcement tension and the general performance of the wall. The result indicated that the horizontal displacement increased from the bottom of the wall to the top with a maximum deflection of 1.5% of the wall height at the end of the construction. They also found that the friction was mobilized at the soil-block interface, and backfill vertical stress was transferred to the block.

Yang et al. (2014) studied the 17 m high two-tiered geogrid-reinforced soil wall backfilled with a soil-rock mixture. Their study involved field instrumentation to measure lateral earth pressures, reinforcement strains, and facing displacements. Their results showed that soil-rock mixtures with a rock content of less than 30% could be effectively used as backfill material with proper attention to compaction quality, geogrid interaction, and installation damage. It was also observed that lateral earth pressures varied between the tiers, with higher pressures developing in the lower portion of the upper. Their results also showed that the reinforcement strains were small, and post-construction lateral displacements ceased after nine months, indicating stable long-term performance.

Balakrishnan and Viswanadham (2016) studied the performance of geogrid reinforced soil walls with marginal backfills using centrifuge model tests. They investigated the effects of geogrid stiffness and the moisture content of backfill on wall deformations. Their results showed that walls reinforced with lower stiffness geogrid layers experience excessive deformations and pullout failures, especially in wet conditions, which can be mitigated with higher-stiffness geogrids and drainage provision.

Vahedifard et al. (2017) investigated the resilience of MSE walls constructed with marginal backfill under extreme precipitation events through numerical modeling. Their study assessed the hydromechanical response of MSE walls to both historical and projected rainfall intensity-duration-frequency (IDF) curves in Seattle. Their result revealed that future precipitation scenarios lead to significantly higher deformations and increased reinforcement loads than baseline scenarios. Their findings showed that site-specific assessments are required when using marginal backfills to adapt infrastructure to a changing climate.

Bui Van et al. (2017) investigated the hydrological behavior of MSE walls using marginal soils with geocomposites as drainage systems. They used numerical simulations to evaluate the influence of unsaturated flow properties and hydraulic conductivity on the stability and phreatic surface levels in MSE walls. Their results indicated that the hydraulic conductivity of the upstream soil and geocomposite drainage capacity play critical roles in controlling water movement and phreatic surface elevation within the protected zone.

Palmeira et al. (2019) investigated the influence of tensile strains and confinement on the filtration opening size (FOS) of nonwoven geotextiles. Their study demonstrated that tensile strain increases the pore size of geotextiles under uniaxial and equal biaxial tension, which was counteracted by confinement, reducing the FOS regardless of the tensile strain. Their results also showed that the degree of pore size change depends on the strain condition and the geotextile's thickness.

Kilic et al. (2021) studied the seismic performance of geosynthetic reinforced retaining walls backfilled with cohesive soil. Their results indicated that walls with cohesive backfills performed better than those with granular backfills, with significantly lower displacements under similar seismic conditions. The cohesion in the backfill also reduced reinforcement strain without compromising load transfer efficiency between geogrids and soil. Their results also showed that the reinforcement length ranged from 0.6H to 0.8H (H: height of the wall) for granular backfill, which was satisfactory for the cohesive backfill as well.

Yang et al. (2023) investigated the performance of geosynthetic-reinforced soil (GRS) walls with marginal backfill subjected to heavy rainfall through a series of model tests. Their results showed that including sand cushions with reduced reinforcement spacing significantly enhanced the wall's stability by effectively delaying water infiltration, reducing porewater pressure, and improving the soil-reinforcement interface's shear strength. Their study also highlighted the necessity of robust hydrological and geotechnical assessments for optimal wall performance under extreme weather events.

2.3 GRS Bridge Abutments

Tatsuoka et al. (2007) introduced the GRS integral bridge, a novel design combining geosynthetic-reinforced soil (GRS) walls with full-height rigid (FHR) facings and an integral bridge structure. This system eliminates the need for girder support, improving cost-efficiency, seismic performance, and long-term serviceability. Laboratory and shaking table tests demonstrated that connecting reinforcement layers to the facing significantly reduces residual settlement and prevents structural damage under thermal and seismic cyclic loading. Compared to conventional gravity-type and integral bridges, the GRS integral bridge exhibited superior dynamic stability and minimal deformation due to its integrated structural behavior.

Abu-Farsakh et al. (2019) conducted a detailed finite element parametric study to assess the performance of Geosynthetic Reinforced Soil–Integrated Bridge Systems (GRS-IBS) under service loading. Using PLAXIS 2D, the study evaluated the effects of abutment height, span length, reinforcement spacing, and stiffness on lateral facing deformation, reinforcement strain, and potential failure zones. Results showed that larger abutment heights and longer spans significantly increased lateral displacements and reinforcement strain. While increasing reinforcement stiffness reduced strain, its effect diminished beyond a certain threshold. Reinforcement spacing consistently influenced performance, with closer spacing providing better confinement. The failure surface was a hybrid of punching shear and Rankine failure envelopes, originating beneath the footing and extending downward, a more accurate representation than conventional assumptions.

Xu et al. (2020) proposed a limit analysis (LA) method using a y-shaped failure mechanism to evaluate the bearing capacity and failure surface geometry of geosynthetic-reinforced soil (GRS) bridge abutments. The analytical model was validated against numerical simulations and experimental results, showing significantly better agreement than traditional limit-equilibrium-based design methods. Their findings indicated that failure surfaces in GRS abutments often exhibit a compound shape, originating from the heel and toe of the footing, unlike the simplified vertical or bilinear failure planes assumed in current guidelines. The study also confirmed that reinforcement strength, spacing, and abutment geometry (e.g., setback distance and facing inclination) have substantial effects on bearing capacity and failure geometry. By incorporating both pullout and rupture mechanisms, the method can identify governing failure modes and provide more accurate predictions for internal stability analysis, offering critical insights for improving the reliability of GRS bridge abutment design.

Hatami and Boutin (2022) conducted full-scale tests on GRS bridge abutments to compare the performance of open-graded and well-graded backfill materials. Both models met FHWA serviceability limits, but the well-graded backfill showed stiffer behavior with smaller settlements and facing deformations, especially at service loads. However, the open-graded fill was easier and faster to compact, offering practical advantages during construction. Despite performance differences, both fill types were deemed effective for GRS abutments when properly compacted.

Jia et al. (2024) investigated dynamic soil stress distribution in GRS bridge abutments using reduced-scale models with well-graded sand and biaxial geogrids under staged cyclic traffic loading. Results showed that stress accumulation was most pronounced near the top of the wall, while reinforcement spacing had minimal influence on vertical stresses. In contrast, cyclic load amplitude had the strongest effect. Closer reinforcement spacing increased lateral confinement and led to higher dynamic lateral stresses. The study also revealed that FHWA and AASHTO design methods underestimated soil stresses under cyclic loading, underscoring the need for more accurate predictive approaches in GRS abutment design.

2.4 Summary

The above literature review is summarized and classified in Tables 2.1 through Table 2.3 according to the type of soil and reinforcement used, tests carried out, and findings in each study. It can be concluded that none of the above-mentioned literature reviews include extensive studies on using marginal soil as a backfill and any design considerations for GRS bridge abutment with marginal soil, which is the focus of this study.

Table 2.1 Literature review summary on pullout tests and bearing capacity

Authors (Year)	Type of Material		Structure/Test Setup	Approach	Type of test	Finding
	Soil	Reinforcement				
Lee et al. (1999)	Sand & Clay	Geotextile	Loading on foundation models	FEA and model tests	Bearing capacity	Geotextile reinforcement increased bearing capacity, reduced settlement, and optimized sand layer thickness for footings.
Abu-Farsakh et al. (2006)	Marginal silty clay soil	Geosynthetics	MSE walls	Field and lab tests	Pullout tests	Marginal silty clay backfills showed adequate pullout resistance; higher strain values in weak geogrids.
Kumar et al. (2007)	Sand	Geogrid (Multiple layers)	Loading on foundation models	Model tests	Bearing capacity	Reinforcing strong top layers enhanced footing stability and bearing capacity by up to 4 times.
Yoo et al. (2007)	Weathered granite soil	Geogrid, Geotextile, Composite	Pullout test apparatus	Model tests and FDA	Pullout tests	Composite reinforcement had high tensile resistance and good drainage properties.
Shivashankar & Jayaraj (2013)	Granular beds over weak soil	Prestressed reinforcements	Loading on foundation models	Model tests	Bearing capacity	Improvement of BCR depended on bed thickness, prestress level, and number of reinforcement layers.
Esmaili et al. (2014)	Marginal soils	Geotextile	MSE walls	Model tests	Pullout tests	Moisture-induced suction reduction led to 42% reduction in pullout resistance; Moisture Reduction Factor was developed.
Abdi & Mirzaeifar (2017)	Granular soil	Geogrid	Pullout test apparatus	Model tests	Pullout tests, PIV, FEA	Larger grain size and non-uniform soils improved pullout forces and interface interaction.

Authors (Year)	Type of Material		Structure/Test Setup	Approach	Type of test	Finding
	Soil	Reinforcement				
Mirzaalimohammadi et al. (2019)	Sand	GGB, GCP	Modified direct shear apparatus for pullout test	Lab tests	Pullout tests	Added components (GGB, GCP) improved pullout resistance by 37-46%.
Mirzaeifar et al. (2022)	Sand	Geogrid	Pullout test apparatus	Model tests	Pullout tests & PIV	Granular encapsulation enhanced pullout resistance, especially under wet and high stress conditions.

Table 2.2 Literature review summary on MSE walls with marginal soil backfills

Authors (Year)	Type of Material		Structure/Test Setup	Approach	Type of test	Finding
	Soil	Reinforcement				
Sandri (2005)	Marginal soils	Geosynthetics, drainage composites	MSE walls	Construction challenges discussion	Seepage, pore pressure risks	Risks in using marginal fills mitigated with drainage systems such as geosynthetics and composites.
Hatami et al. (2012)	Marginal soils	Geotextile	MSE walls	Large-scale tests	Pullout tests	Moisture content reduced pullout capacity by 37-47%, Moisture Reduction Factor was introduced.
Yoo (2013)	Marginal soils	Geosynthetic	MSE walls	Numerical modeling	FEA	Reinforced walls showed significant displacement and load increases during rainfall.
Riccio et al. (2014)	Clayey-Sand	Geogrid	MSE wall	Field tests	Horizontal displacement tests	Soil compaction affected wall performance; maximum horizontal deflection was 1.5% of wall height.

Authors (Year)	Type of Material		Structure/Test Setup	Approach	Type of test	Finding
	Soil	Reinforcement				
Balakrishnan & Viswanadham (2016)	Marginal soils	Geogrid	MSE walls	Centrifuge model tests	Wall deformation tests	Lower stiffness geogrids caused excessive deformations and failures in wet conditions; higher stiffness and drainage reduced risks.
Vahedifard et al. (2017)	Marginal soils	Geogrids	MSE walls	Numerical modeling	Hydromechanical response tests	Increased deformations and reinforcement loads during extreme precipitation events; site-specific adaptation needed for future climate scenarios.
Bui Van et al. (2017)	Marginal soil	Geocomposites	MSE walls	Numerical simulation	Hydrological stability tests	Upstream soil conductivity and drainage capacity influenced water movement and stability.
Kilic et al. (2021)	Clayey Sand	Geosynthetic	MSE walls	Seismic model tests	Seismic performance	Cohesive backfill had lower displacement under seismic loading; cohesion enhanced load transfer.
Yang et al. (2023)	Marginal soil	Geosynthetic & sand cushion	MSE walls	Model test	Hydrological stability tests	Sand cushions reduced water infiltration; lower pore pressures and improved interface shear strength.

Table 2.3 Literature review summary on GRS bridge abutments

Authors (Year)	Material Examined		Structure/Test Setup	Approach	Type of test	Finding
	Soil	Reinforcement				
Tatsuoka et al. (2007)	Sand	Geosynthetics	GRS bridge abutments	Lab & shake table tests	Seismic & thermal tests	FHR facing reduced settlement under cyclic loads; superior dynamic behavior vs. conventional systems.

Authors (Year)	Material Examined		Structure/Test Setup	Approach	Type of test	Finding
	Soil	Reinforcement				
Abu-Farsakh et al. (2019)	Open graded aggregates-	Geosynthetic	GRS bridge abutments	PLAXIS 2D	Wall behavior	Close spacing and higher stiffness improved strain control; identified hybrid failure surfaces.
Xu et al. (2020)	Coarse aggregate	Geosynthetic	GRS bridge abutments	Limit Analysis	Failure surface	Y-shaped failure surface better than bilinear assumption; validated via experiments and FEM.
Hatami & Boutin (2022)	Well-graded & Open-graded aggregates	Geosynthetic	GRS bridge abutments	Full-scale tests	Wall behavior	Well-graded fill reduced settlement and deformation more effectively; both fills met serviceability.
Jia et al. (2024)	Well-graded sand	Biaxial geogrid	GRS bridge abutments	Cyclic loading test	Dynamic stress	Higher stress at the wall top; reinforcement spacing increased lateral stress; existing guidelines underestimated stress.

3. Hypotheses, Objectives, and Goals

3.1 Hypotheses

The hypotheses for this study are:

1. Marginal soil with fines content greater than 12% can also be used as backfill material as long as a tightly-spaced reinforcement design is used for GRS bridge abutments.
2. Marginal soils could also be considered for GRS bridge abutments with tightly spaced, but nonuniform reinforcement spacing due to drainage layers or other considerations. Such GRS bridge abutments with marginal soil backfill can still provide satisfactory performance in service conditions.

3.2 Objectives

This study aims to explore several key areas concerning the performance and stability of GRS bridge abutments under varying conditions.

First, it seeks to determine how the stability of GRS bridge abutment is influenced by using marginal soil, recognizing that water content can significantly affect soil behavior and, consequently, abutment stability.

Secondly, the research intends to evaluate the mechanical performance of GRS bridge abutments constructed with marginal soil, specifically focusing on how variations in soil type impact these structures.

Lastly, the study will assess the effect of footing location behind the facing of GRS bridge abutments backfilled with marginal soil. Through these objectives, the research aims to provide insights into the factors that could influence the stability and performance of GRS bridge abutments with marginal backfills.

3.3 Goal

The primary goal of this research is to contribute to advancing design and construction practices for GRS bridge abutments. By focusing on efficiently utilizing marginal soils, the study aims to provide insights that could lead to improved guidelines. These enhanced guidelines could ensure that using less-than-ideal soil types does not compromise the structural safety and integrity of GRS bridge abutments. Through this effort, the research seeks to support the engineering community in developing more sustainable and cost-effective solutions for GRS bridge abutment construction, thereby extending the potential applications of these structures in various geotechnical engineering projects.

4. Methodology

4.1 GRS Abutment Models

This research is part of a larger, ongoing project focused on the performance evaluation of Geosynthetic Reinforced Soil (GRS) bridge abutments that could be constructed with marginal soil backfills. In this initial phase of the study, three model abutments were constructed to serve as baseline cases for the broader study: (1) Model 1, a control GRS model with clean sand used as backfill; (2) Model 2, same as Model 1 but backfilled with marginal soil; and (3) same as Model 2 soil but loaded closer to its facing (Figure 4.1). The dimensions and configurations of the three GRS models are shown in Figure 4.2 and summarized in Table 4.1.

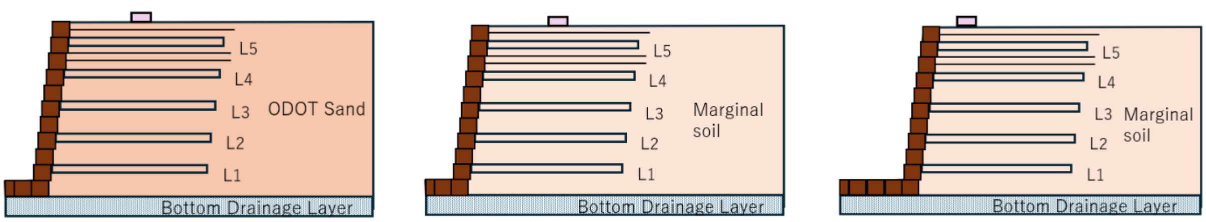

(a) Model 1 (b) Model 2 (c) Model 3

Figure 4.1 GRS bridge abutment configurations tested in this study. Note: (1) L1, L2, … L5 represent the primary reinforcement layers, (2) the three bold horizontal lines inside the model indicate additional reinforcement layers under the strip footing load.

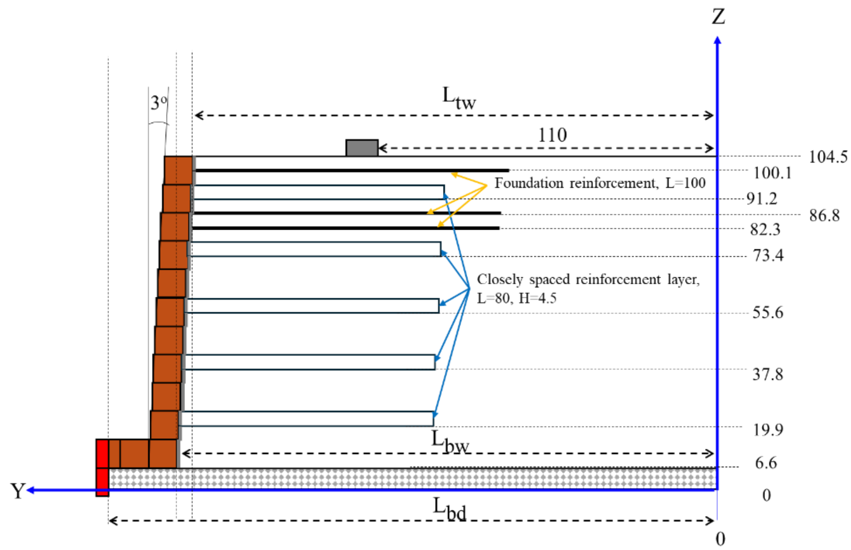

Figure 4.2 Schematic diagram of a constructed model GRS bridge abutment. Note: Abutment height was the same in all models

Table 4.1 Dimensions of model abutments (m)

Parameter	Models 1 & 2	Model 3
Backfill width at the bottom(L_{bw})	1.70	1.50
Backfill width at the top (L_{tw})	1.653	1.53
Length of bottom drainage layer (L_{bd})	1.921	
Height of bottom drainage layer	0.066	
Total abutment height	1.045	

Each model abutment was initially subjected to the allowable service load defined by FHWA guidelines for bridge abutments (4,000 lb/ft² ≈ 190 kPa), and then further loaded until visible signs of failure, typically surface cracking, were observed. However, due to the confinement of the models within the test box, the final loading phase is expected to have mobilized not only the models but also the test box itself. As a result, data collected beyond the service load is considered supplementary and is included for reference in future research.

Model 1 underwent three phases of testing. The first phase was halted due to a localized failure caused by a narrow (i.e. 100 mm-wide) strip footing that was initially used and led to punching failure at the top of the backfill. Subsequently, the footing width was doubled. In the second phase, the model was loaded up to the serviceability limit and subsequently larger loads, but the test was terminated due to a hydraulic jack malfunction caused by oil leakage. After resolving the mechanical issue, a third phase was conducted. The model was loaded to an ultimate value, and the test was terminated upon the appearance of surface cracks at 1000 mm from the back of the facing timber.

Model 2 also underwent three testing phases but all using the wider footing. During the first phase, the model abutment was loaded to the serviceability limit and then to the final load, at which point cracks were observed around the footing area, and the test was halted. The second phase aimed to evaluate the model abutment's elastic response, while the third phase involved an attempt to increase the model's moisture content and reload the previously tested model to both the serviceability and ultimate load levels. An attempt was made to significantly increase the moisture content of Model 2 to achieve saturated conditions. However, full saturation was not achieved, as the water content did not increase as intended due to time constraints. Although data were collected for this phase, they were not analyzed in the present study and are retained as supplementary information for future research. This third phase was terminated once the previously observed cracks reappeared.

Model 3 was subjected to a single phase of testing. It was loaded up to the serviceability limit and then to an ultimate load, at which point surface cracks were observed at 1.0 m from the back of the timber facing, marking the end of the test.

All test phases and observations of the study are summarized in Table 4.2.

Table 4.2 Test phase summary for model abutments

Model	Test Phase	Nominal footing Width (mm)	Final Load		Reason for aborting the test
			(kPa)	(kN)	
1	1 (Sand backfill)	100	277	21.33	Narrow footing, start of punching failure
	2 (Sand backfill)	200	482	70.86	Hydraulic jack oil leakage
	3 (Sand backfill)		1,418	208.40	Final load
2	1 (Marginal soil backfill with water content OMC +3%)		1,800	264.66	Final load
	2 (Marginal soil backfill with water content OMC +3%)		575	84.46	Unloading and reloading to compare with a subsequent wet backfill model
	3 (Marginal soil backfill with an attempt to increase the water content)		2,122	311.90	Final load
3	1 (Footing placed near the facing)		2,038	299.56	Final load

For the purposes of this study, the following test phases were selected for analysis: Model 1 Phase 2, Model 2 Phase 1, Model 2 Phase 2, and Model 3. These will hereafter be referred to as follows: Model 1 (control case with sand backfill), Model 2 (marginal soil backfill at OMC + 3% water content), Model 2W (marginal soil backfill with increased water content), and Model 3 (footing placed near the facing), respectively.

4.2 Material Properties

4.2.1 Backfill Soil and Drainage Materials

The test utilizes two soil types for backfill in this study. Sand was used as a backfill for Model 1. As mentioned in the introduction, the standard for marginal soil is that it contains at least 15% fine particles. Since the silty sand obtained for this study alone did not contain at least 15% fine particles, lean clay was mixed in to create a mixture that contained at least 15% fine particles. The mixing ratio of silty sand and lean clay was determined in preliminary experiments to be 85% silty sand and 15% lean clay, leading to 24.7% fines for Model 2 marginal soil as backfill. For Model 3, previously used marginal soil was reused as backfill material. Physical and mechanical soil property tests were performed on these soils in accordance with ASTM D6913 to determine the soil gradation and fines content. Figure 4.3 shows the gradation curves from sieve analysis for the soil sample. The compaction test was performed in accordance with ASTM D698 to determine the optimum moisture content of sand and marginal soil (Figure 4.4). The direct shear test and hydraulic conductivity tests were performed in accordance with ASTM D3080 and ASTM D2434, respectively, to determine the cohesion and friction angle, and permeability of sand and marginal soil. Table 4.3 shows the properties of these soils based on laboratory tests at OU in accordance with the related ASTM standards. The direct shear test data tabulated below is at OMC for sand and OMC+3% for marginal soil.

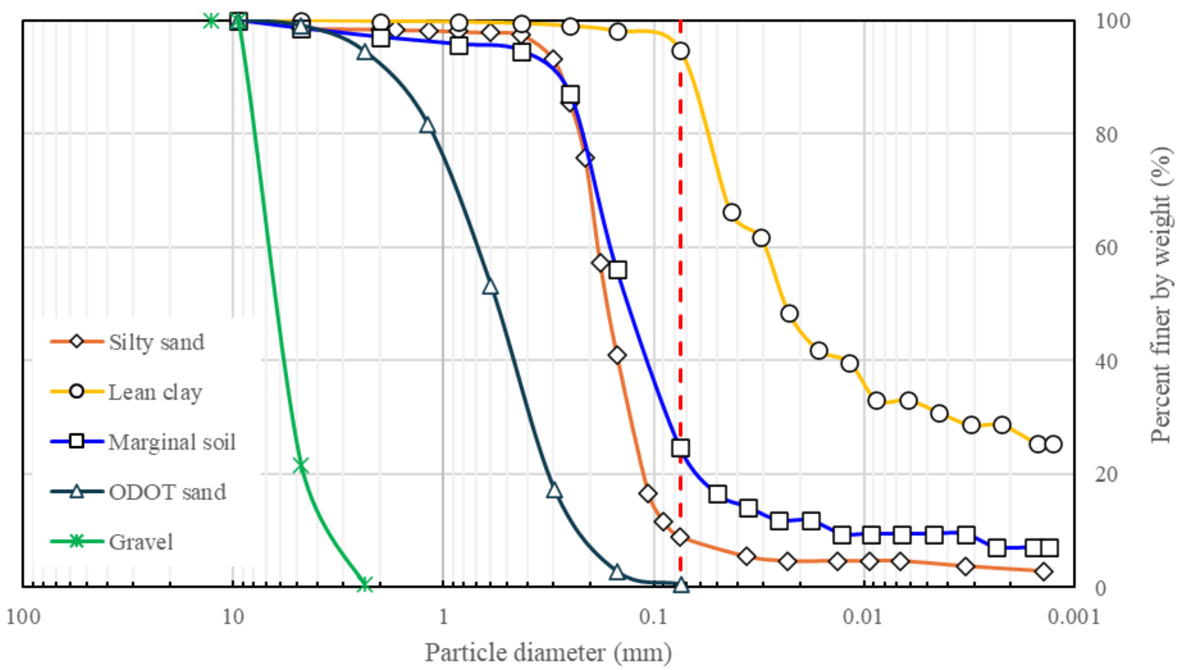

Figure 4.3 Gradation curve for the soil samples used as backfill and drainage materials. Note: The red vertical broken line shows the location of sieve number #200

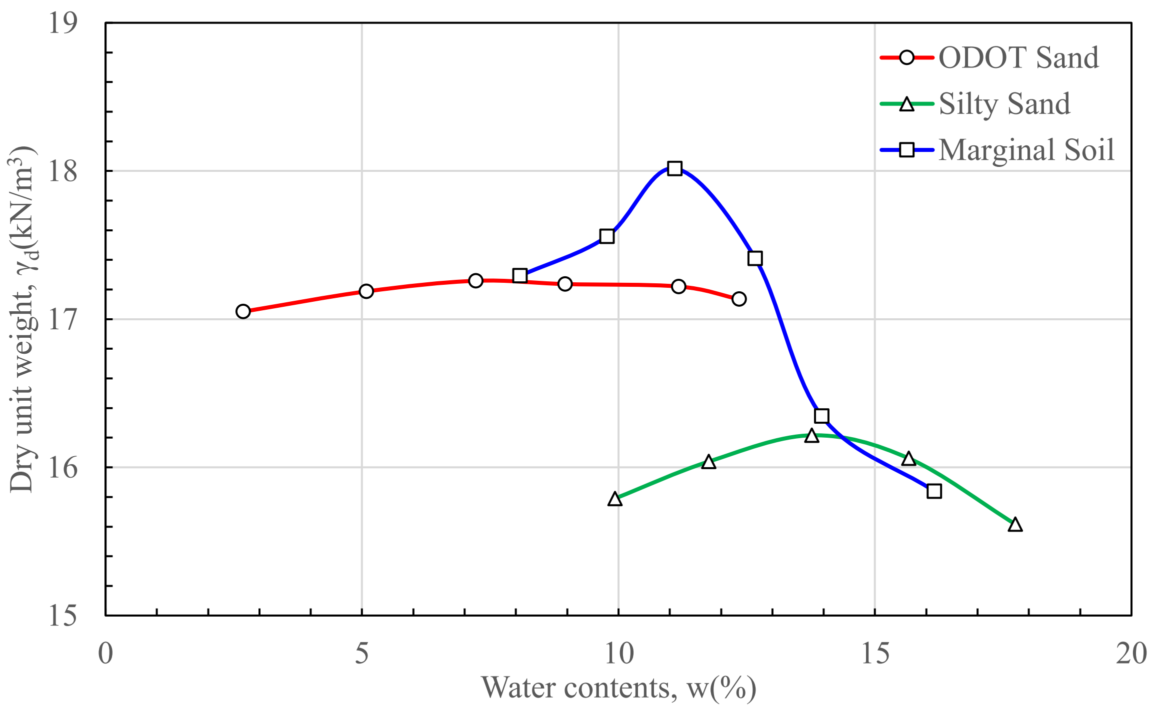

Figure 4.4 Compaction test results for the backfill soil

Table 4.3 Physical and mechanical soil properties

		Unit	Model 1	Marginal Backfill Components		Models 2 & 3	Bottom layer	ASTM
Soil Property			ODOT-Fine Sand	Silty sand	Lean clay	Marginal soil (15% clay mixed)	Gravel	
Classification	Unified		SP	SP-SM		SM	GP	D2487
	AASHTO		A-1-b	A-3(0)		A-2-4(0)	A-1-a	
Liquid limit, Plastic limit		%	NP,NP	NP,NP	19, 32	NP,NP	NP,NP	D4318
Specific gravity				2.651				D854
Sand, silt, clay		%	99.5,0.5,0	89.7,4.7,4.2		75.3,17.6,7.1	25.7,0,0	D6913
Maximum Particle Size		mm	9.5	4.75	2	4.75	9.5	
D60		mm	0.685	0.184		0163	6.817	
D30		mm	0.397	0.128		0.084	5.021	
D10		mm	0.235	0.080			3.575	
Cu			2.9	2.3			1.91	
Cc			1.0	1.1			1.03	
Passing	#4	%	99.1	98.6	100	98.6	25.7	
	#200	%	0.5	8.9	94.8	24.7	0.0	
Maximum dry unit weight		kN/m^3	17.22	16.21	16.92	18.40	-	D698
Optimum moisture content		%	8.0	14.0	17.1	11.1	-	

	Unit	Model 1	Marginal Backfill Components		Models 2 & 3	Bottom layer	ASTM
Cohesion	kPa	7.4	-	-	9.7	-	D3080
Internal friction angle	deg.	38.9	-	-	35.9	-	
Permeability	m/s	4.0×10^{-4}	-	-	3.09×10^{-6}	-	D2434

4.2.2 Reinforcement

The model tests utilized a woven polypropylene (PP) geotextile, specifically Mirafi HP570, for the closely spaced reinforced layer (Figure 4.5a) and foundation reinforcement (Figure 4.5b). The closely reinforced geotextile layer with a length of 800 mm and a foundation reinforcement with a length of 1,000 mm were divided into three sections with a width of 140 mm, 400 mm (center), and 140 mm. A folded 10 mm thick needle-punched nonwoven geotextile composed of polypropylene fibers was used for chimney drainage (Figure 4.5) (Mirafi 140N). Table 4.2 shows the properties of HP570 woven geotextile and 140N nonwoven geotextile.

(a) (b)

Figure 4.5 Geotextiles used in Model abutments; (a) geotextile used as a closely spaced reinforcement layer, (b) geotextile used as a foundation reinforcement. Note: the chimney drainage layer is highlighted with a red rectangle

Table 4.4 Mechanical properties of geotextiles

<table>
<tr><th rowspan="3">Mechanical Properties</th><th rowspan="3">Unit</th><th colspan="2">Mirafi HP570</th><th colspan="2">Mirafi 140N</th></tr>
<tr><th colspan="4">Minimum Average Roll Value</th></tr>
<tr><th>Machine Direction</th><th>Cross-Machine Direction</th><th>Machine Direction</th><th>Cross-Machine Direction</th></tr>
<tr><td>Tensile Strength (ultimate)</td><td>kN/m</td><td>70</td><td>70</td><td>-</td><td>-</td></tr>
<tr><td>Tensile Strength (at 5% strain)</td><td>kN/m</td><td>35</td><td>43.8</td><td>-</td><td>-</td></tr>
<tr><td>Grab Tensile Strength</td><td>N</td><td>-</td><td>-</td><td>534</td><td>534</td></tr>
<tr><td colspan="2"></td><td colspan="4">Minimum Roll Value</td></tr>
<tr><td>Permittivity</td><td>sec^{-1}</td><td colspan="2">0.4</td><td colspan="2">1.7</td></tr>
<tr><td>Permeability</td><td>cm/sec</td><td colspan="2">0.05</td><td colspan="2">-</td></tr>
<tr><td colspan="2"></td><td colspan="4">Maximum Opening Size</td></tr>
<tr><td>Apparent Opening Size (AOS)</td><td>mm</td><td colspan="2">0.6</td><td colspan="2">0.212</td></tr>
</table>

4.2.3 Facing

The model abutment facing consisted of 11 courses of blocks, each comprising three separate columns made of 89 mm × 89 mm timber sections. Each course included three timber lengths: 164 mm (left and right) and 400 mm (center). To reduce friction at the timber–vinyl sheet interface, a one-inch-thick foam layer was attached to the outermost part of the facing, flush with the timber dimensions (Figure 4.6a and 4.6c). Additionally, the inner surfaces at timber-to-timber junctions were coated with wax to minimize internal friction. All timber elements used in the tests were coated with waterproof paint to prevent moisture absorption.

Geotextile layers used in the closely spaced reinforcement layer were attached to the timber using a stapler as shown in Figure 4.6b. For the top geotextile layer, a 2-inch-square patch was glued at a designated location to provide additional support for screwing in the wire potentiometer cable.

(a)

(b)

(c)

Figure 4.6 Geotextile stapled to the facing; (a) side timber with a foam (b) center timber (c) arrangement of all three timbers for one step of facing

4.3 Test Equipment

4.3.1 Test Box

A portable test box of size 2,000 mm (L) × 780 mm (W) × 1,200 mm (H) with an integrated loading frame was used in this experiment, which was already available in the Geosynthetics Lab at Fears Structural Laboratory (Figure 4.7). The side walls of the box were covered with 30 mm thick polycarbonate glass to allow observation and measurement of the model deformation. The polycarbonate thickness and the steel columns were designed in such a way that the side wall remains mostly rigid during loading. Thin plexiglass sheets of 5 mm were placed over the inner side walls to protect the main polycarbonate glass from getting scratched during the construction and compaction of the model. Horizontal lines spaced at 45 mm were drawn on the plexiglass sheet to represent lift thickness for backfill material. Also, a vinyl sheet of 1,900 mm by 1,100 mm was taped on the plexiglass, and mineral oil was applied to reduce side wall friction with the backfill. After that, another same-size vinyl sheet was added, which was cut into three sections, the middle part having the same width as the footing. The first section is the length from the back of the box to the back of the footing. Both inner sides of the box had vinyl sheets attached using masking tape during construction, which was removed later before testing started. On the back side of the test box, many holes were already there from before, so a vinyl sheet with holes was used for passing the potentiometer wires, and the rest of the holes were sealed with silicone sealant to prevent backfill from leaking out (Figure 4.7). The wire potentiometer cables were extended using thin steel cables, which were inserted through designated holes in the back of the test box and passed through pre-measured hollow tubes. One end of each steel cable was connected to the wire potentiometer mounted on the back shelf, while the other end was fitted with a circular ring that allowed it to be securely screwed into the geotextile. The circular ring served to prevent the cable from slipping out of the tube during testing. The hollow tube acted as a guide, enabling smooth and unrestricted sliding of the wire potentiometer cables as strain developed in the geotextile.

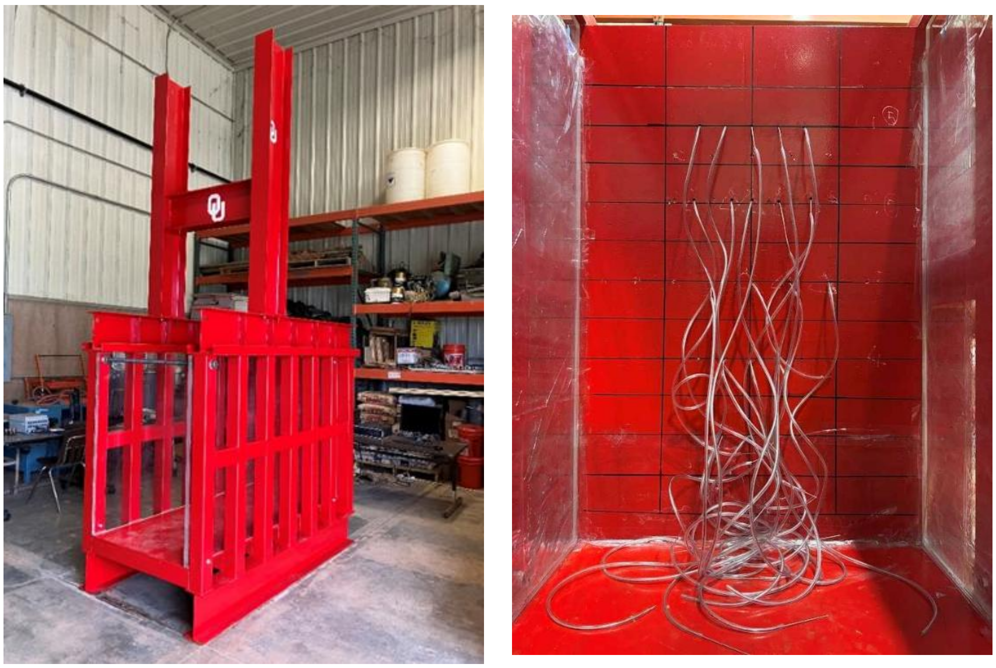

Figure 4.7 Test box at the Geosynthetics Laboratory at Fears for GRS bridge abutment model tests

4.3.2 Loading Device and Footing

A 22-ton, 150-mm stroke, "ENERPAC RC 506" of weight 22.3 kg manual control hydraulic cylinder connected to a "ENERPAC P80" pump, together with a vertical loading column (supported on the top beam of the test box) as shown in Figure 4.8, was used to apply a vertical line load on the models. A 710 mm (L) x 100 mm (W) x 50 mm (H) strip steel footing was used for the Model 1 phase 1, for the remaining phases of Model 1, Model 2, and Model 3 additional strip footing of 770 mm (L) x 100 mm (W) x 50 mm (H) was used along with the previously used footing.

Figure 4.8 Loading arrangement used in the model abutments with the zoomed-in view on the right side

4.4 Preparation of Backfill Materials

Silty sand, Clay, and ODOT sand, representing a select fill for the control case, and gravel for the bottom drainage layer, were stored in the northern area of the Fears Lab at OU, and a plastic tarp was placed on the ground to cover these soils.

4.4.1 Processing Gravel

All model abutments consisted of a bottom drainage layer to allow water to seep through it. The amount of gravel needed for the bottom drainage layer (m_{need}) was calculated using Equation 4.1. A total of 142 kg of gravel was used to achieve a compaction degree of 90%.

$$m_{need} = V \times \rho_d \, at \, DC \tag{4.1}$$

Where:

V = Volume of lift (Height of layer x Width x Length) (cm^3)

ρ_d at DC = Dry density of gravel at the desired degree of compaction (g/cm^3)

4.4.2 Sand for Model 1

For the first Model Abutment, ODOT sand was mixed with predetermined water contents of 5%, 6%, 7%, and 8%. The amount of soil required for each lift (m_{need}) was calculated by considering the volume of that lift, the specified water content ratio (w), and the dry density (ρ_d) of the soil mix, as shown in Equation 4.2.

$$m_{need} = V \times \frac{\rho_d \, at \, DC}{(1 + \frac{w_{target}}{100})} \tag{4.2}$$

Where:

w_{target} = desired water content of soil or target water content (%)

Equation 4.2 determined the quantity of wet soil needed at the target water content. Following this, Equations 4.3 and 4.4 were applied to calculate the required amounts of dry soil and water, respectively, for that amount of wet soil:

$$m_{dry} = \frac{m_{wet}}{\left(1 + \frac{w}{100}\right)} \tag{4.3}$$

$$m_{water} = m_{wet} - m_{dry} \tag{4.4}$$

Where:

m_{wet} = mass of wet soil (kg)

m_{dry} = mass of dry soil (kg)

m_{water} = mass of water (kg)

w = current water content (%)

Since natural soil contained some moisture, the process of mixing soil to target water content began by placing a soil mass exceeding m_{need} into the concrete mixer and mixing it thoroughly. The initial water content of the soil was then determined from the ASTM D4643-17 microwave oven test method. Using this value, Equations 4.3 and 4.4 were used to determine the dry soil mass and water mass contained within the mixture. Finally, Equation 4.5 was used to calculate how much more water to use in order to reach the specified moisture content and that amount was added to the mixture. After mixing for 8 to 10 minutes to achieve a uniform consistency, the required amount of soil for the lift (m_{need})was measured and divided into four buckets. Each bucket was then sealed with a lid and labeled with the corresponding lift number.

$$m_{add} = \frac{w_{target} * \mathrm{m}_{dry}}{100} - m_{water} \tag{4.5}$$

Where:

m_{add} = mass of water needs to be added (kg)

The calculation and process outlined above were followed to determine the amount of soil needed per lift for a 95% degree of compaction. The soil mixing process took approximately 6 to 8 days. A total of eighty-eight 5-gallon buckets were used to store the wet soil, which was sealed and kept for more than 24 hours to allow moisture equilibrium.

4.4.3 Marginal Soil for Model 2

The backfill soil required for the second model abutment was prepared by mixing 85% silty sand and 15% clay at a water content of 14% (OMC + 3%) to achieve a compaction degree of 90%. The clay was first air-dried and crushed into crumbles using a crusher, and the water content of the crushed clay (w_{clay}), along with the amounts of dry clay and water in the clay, were calculated using Equations 4.3 and 4.4. The prepared clay was afterward kept in airtight containers to maintain moisture.

The quantity of marginal soil needed for each lift (m_{need}) was calculated using Equation 4.2. Following this calculation, the quantities of dry soil and water needed to reach the target water content were determined. Silty sand, weighing 20 kg plus 0.85 times the required dry mass of marginal soil, was mixed in the concrete mixer until it reached a homogeneous color. Subsequently, the water content of the silty sand mixture was measured, and the actual dry mass of silty sand and water content present were determined. Excess silty sand exceeding 0.85 times the required dry mass of marginal soil was then removed from the mixture.

Next, the dry mass of clay, calculated as 0.15 times the dry mass of marginal soil, needed to be added to the concrete mixer. Since the clay had its initial water content, the amount of moist clay required in the mixture was calculated based on this initial moisture content using Equation 4.6. This moist clay was then thoroughly mixed with the silty sand in the concrete mixer until a homogeneous color was achieved. The water content of the combined mixture was measured again, and additional water needed to reach the target water content of 14% was calculated using Equation 4.5. This calculated water amount was added to the mixture and mixed thoroughly until uniformity was observed. Then the mixed soil A total of 2,418 kg of marginal soil was processed for the second model abutment and was stored in 88 sealed 5-gallon buckets for more than 24 hours to ensure moisture equilibrium. The entire soil mixing process for the second model took approximately 8 to 10 days.

$$m_{moist\ clay} = m_{s(clay)} + \frac{m_{s(clay)}\ x\ w_c}{100} \tag{4.6}$$

Where:

$m_{moist\ clay}$ = required mass of moist clay (kg)

$m_{s(clay)}$ = mass of dry clay (i.e. 0.15 x target mass of marginal soil for that lift) (kg)

w_c = current water content of clay (%)

The processing of marginal soil used in constructing the second model abutment is shown in Figure 4.9.

(a)

(b)

(c)

(d)

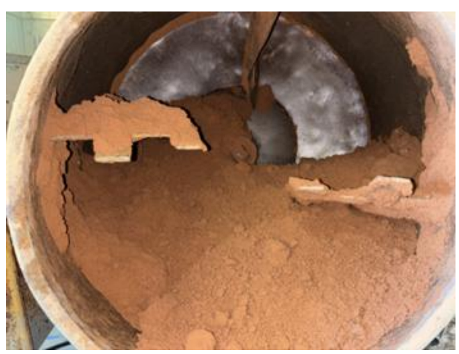

(e)

Figure 4.9 Marginal soil processing for the second model abutment: (a) air drying process of clay, (b) crushing large chunks of clay to smaller particles, (c) crushed soil, (d) silty sand before mixing it with clay, (e) mixed marginal soil to desired moisture content

4.4.4 Marginal Soil for Model 3

For the third model, the same soil used in the second model was reused after air drying. Following the steps outlined in section 4.3.2, the air-dried marginal soil was mixed in the concrete mixer to reach a target water content of 14%. A total of 2,175 kg of soil to achieve a 90% compaction degree was processed and stored in 78 sealed 5-gallon buckets for more than 24 hours to ensure moisture equilibrium. The entire soil mixing process for the third model took approximately 4 to 6 days.

4.5 Construction of Model Abutments

The models were constructed with a timber-facing batter angle of 3 degrees. Two steel beams were screwed into the bottom of the test box to permanently secure the bottom drainage layer and the first timber step, as shown in Figure 4.10a. A 66 mm-thick gravel layer was then placed in two lifts at the bottom of the test box to serve as the drainage layer and was compacted. A 1,920 mm (L) x 780 mm (W) piece of Mirafi HP570 geotextile was placed on top of the gravel as a separator fabric, as shown in Figure 4.10b.

(a) (b)

Figure 4.10 (a) Gravel layer for the bottom drainage layer, (b) separator fabric for the bottom drainage layer. Note: The blue rectangle shows the fixed support

Once the first course of the facing timber was placed inside the test box, the backfill soil for the first lift was added. Before the placement and compaction of each lift, the designated soil was emptied into a large tub and hand-mixed using shovels to ensure uniform moisture distribution. This thoroughly mixed soil was then used for construction (Figure 4.11).

(a) (b)

Figure 4.11 (a) Mixing soil before construction, (b) soil compaction inside the test box

After compacting the first two lifts (i.e., the first timber step), support timber with threaded rods was clamped to the front of the test box to secure the next step of facing timber (Figure 4.12). The facing timbers were placed before each backfill lift was added and compacted. This process of clamping the supporting timber prior to placing each facing timber, followed by soil placement and compaction, was repeated till the end of the construction in each model abutment. In total, the soil was compacted in twenty-two lifts, each being 45 mm thick. During the compaction process, the EC5 sensors were simultaneously installed at their designated positions as per the instrumentation plan (detailed instrumentation plan is provided in Chapter 5).

Figure 4.12 Support timber for facing (front view, side view, and top view)

For the first model, backfill sand was compacted at varying moisture contents: 5% for the first five lifts, 6% for the next five, 7% for the following six, and 8% for the final six lifts. In contrast, the second and third models were compacted entirely at a moisture content of 14%.

Closely spaced reinforcement layers, with dimensions of 680 mm (W) (divided into three sections as explained in Sections 4.1.2 & 4.1.3) × 45 mm (H) × 800 mm (L), were installed in one lift at heights of 199 mm, 378 mm, 556 mm, 734 mm, and 912 mm from the bottom of the test box as shown in Figure 4.2. To construct the closely spaced reinforcement layer, firstly the bottom geotextile with one end attached to facing timber and another free end was laid in place. The free end of the geotextile was then folded upward to form a pocket-like enclosure. Afterward, backfill soil was placed and compacted over the folded geotextile. For each subsequent layer, once the geotextile was laid in place, the wire potentiometer cable was screwed into it (Figure 4.13). After securing the cable, WD-40 lubricant was sprayed inside the hollow tube to reduce friction between the wire potentiometer cable and the tube, allowing smoother movement during straining. Once the cable was properly installed, the free back end of the current geotextile layer was carefully tucked into the folded portion of the geotextile from the previous layer, maintaining continuity in the reinforcement system. This interlocking configuration ensured that the back portion of each layer was enclosed and reinforced by the preceding layer, thereby maintaining a consistent and secure facing throughout the model construction. Wire potentiometers were attached to the top portion of a closely spaced geotextile to measure strain in the geotextile within the model, as described in Chapter 5. A chimney drain layer made of nonwoven geotextile was placed behind the facing timber to complete the drainage system (Figure 4.13).

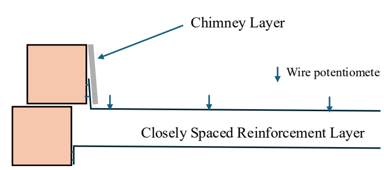

(a) (b)

Figure 4.13 (a) Top view of the drainage geotextile connected to a wire potentiometer, with the drainage chimney layer located behind the facing timber, (b) Representational side view of a closely spaced reinforcement layer

Three additional layers of geosynthetic reinforcement, each 680 mm wide (divided into sections of 140 mm, 400 mm, and 140 mm wide) and 1,000 mm long, were placed at heights of 823 mm, 867 mm, and 1,001 mm from the base of the test box. These foundation reinforcement layers were not connected to the facing.

Water content was measured at different locations during the construction phase. For the second and third tests, the degree of compaction was also measured.

The construction of the first model abutment required 42 person-hours, while the second model required 57 person-hours, and the third model required 42 person-hours.

4.6 Backfill Wetting

To investigate the behavior of the second model under increased moisture conditions, a third phase was conducted for Model 2. After completing the second phase, the loading beam and hydraulic jack were removed. Five plastic buckets were selected, and a 1 mm diameter hole was drilled at the center of each to facilitate controlled water release. These buckets were placed evenly across the top of the model. Each bucket was then partially filled with approximately 25 kg of water (Figure 4.14a,b).

The condition of the model was monitored the following day, and an additional 25 kg of water was added. This process was repeated daily for a week. Once clear water was observed draining into the collection bucket in front of the model abutment (Figure 14.4c), it was assumed that the model had reached a state of partial saturation and could no longer absorb additional water.

(a) (b) (c)

Figure 4.14 (a) Top view of the model abutment setup with buckets used for saturation, (b) front view of the model during the saturation process, and (c) clear water collected in the drainage bucket, indicating partial saturation of the model

4.7 Loading of Model Abutments and Subsequent Deconstruction of the Test Setup

4.7.1 Support Removal

In preparation for the loading stage, the masking tape used to attach the innermost divided vinyl sheets was removed to allow free movement of the model. After the masking tape was removed, the support timbers for the facing were also taken out. The removal of these supports was carried out in a stepwise manner. The top support was removed first, and the facing distance was measured using a Model HS60 Laser Distance Meter and tape measure. After waiting for 10 minutes, the measurement was taken again. Then, the second support was released, and immediately after removal, the facing distance from the same reference point was measured for both facings. This was followed by another measurement after 10 minutes. This process was repeated for all the facings in each of the three model abutments. No movement of the facing in all three model abutments was observed during the removal of the support timbers. Figure 4.15 shows the models before and after removing the support timbers.

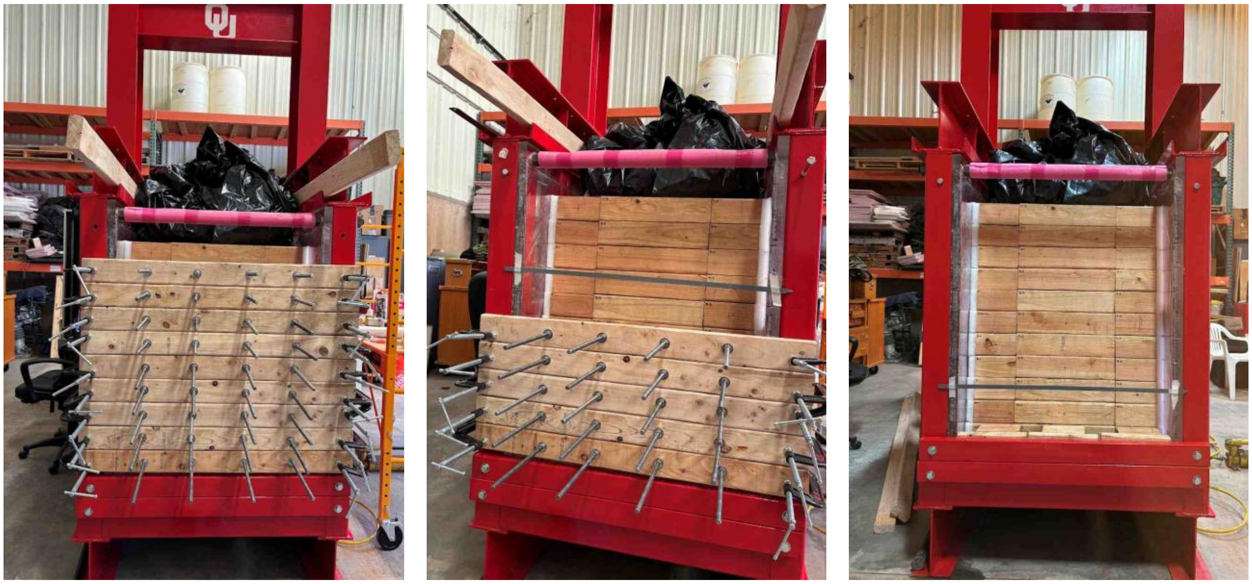

(a) (b) (c)

Figure 4.15 (a) Model abutment with facing support, (b) model abutment during support removal, (c) model abutment after facing support removal. Note: The top of model abutment has plastic tarp secured with wooden timber, to retain the moisture from construction until testing

Once all the facing timbers were removed, wire potentiometers were attached. Each wire potentiometer was first screwed onto a timber block (Figure 4.16a), which was then clamped securely to the front of the text box. The wire from each potentiometer was then hooked to the facing timbers using pre-screwed hooks (Figure 4.16b). This setup ensured accurate measurement of facing displacement while allowing sufficient space for the facing to move freely during model deformation or failure. A special timber assembly was designed to maintain this necessary clearance between the facing and the timbers for the wire potentiometer throughout the loading phase (Figure 4.16c).

(a) (b) (c)

Figure 4.16 (a) Wire potentiometer mounted on a timber block, (b) wire potentiometer wire connected to the facing timbers via pre-screwed hooks, (c) timber block with attached wire potentiometer clamped to the front of the test box

4.7.2 Loading of Model Abutments

Once all the wire potentiometers were attached, a hollow steel section of 710 mm-long, 5 mm-thick, and 100 mm-wide strip footing was placed 1,100 mm away from the back of the test box for Phase 1 of Model 1. For the remaining phases of Model 1, as well as for Model 2 and Model 3, an additional hollow steel section of 770 mm-long, 5 mm-thick, and 100 mm-wide footing was also placed alongside the previously used footing to simulate wider loading conditions. A hydraulic cylinder was positioned at the center of the strip footing to prevent any unwanted tilting during loading. A load cell was then placed on top of the hydraulic cylinder, followed by a vertical loading column (Figure 4.17).

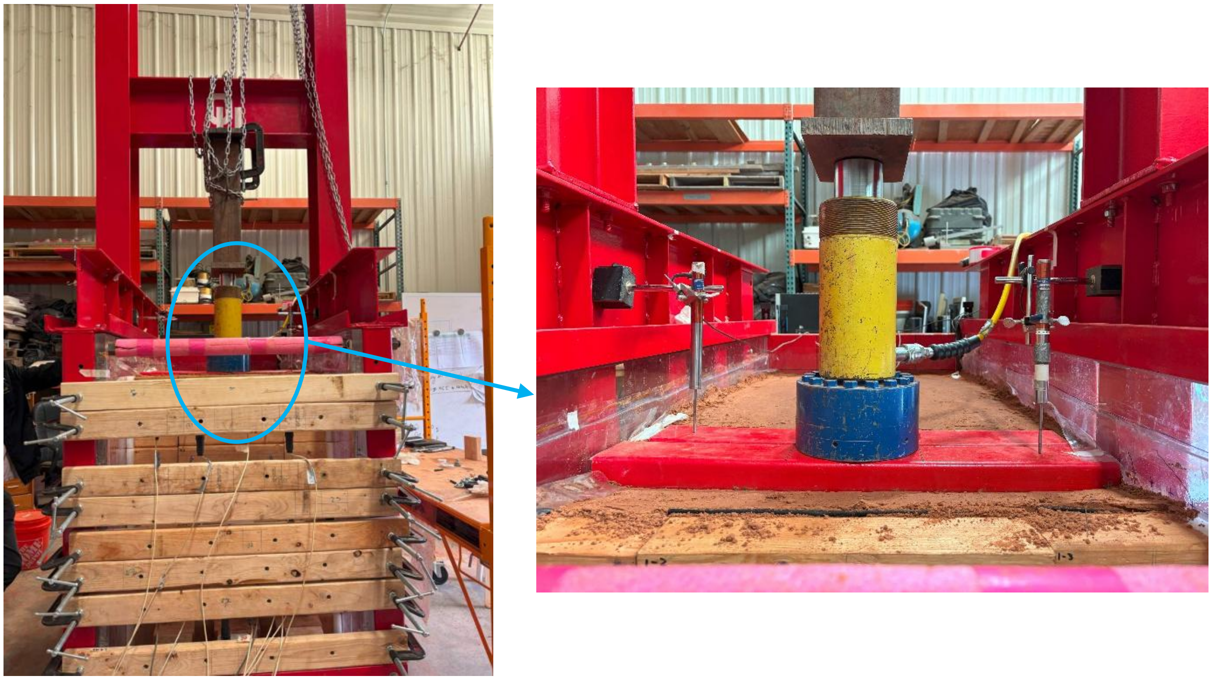

Figure 4.17 Loading arrangement used for model abutments, including the hydraulic jack, load cell, and vertical loading column setup

The loading was applied incrementally, initially in 10 kPa steps up to 240 kPa, and then in 20 kPa increments until a clear indication of failure was observed in the backfill.

4.7.3 Deconstruction of the Test Setup

After completing all the testing phases, the test assembly was carefully dismantled. The process began with removing the surcharge assembly from the top of the test box. For the first model abutment, which was constructed using sand, careful excavation by individual layers was not feasible. Additionally, since the model was left undisturbed for several days before deconstruction, the water content was not measured during excavation.

However, for the second and third model abutments, excavation was performed, lift by lift, as much as possible. During this process, both the water content and unit weight of the soil were measured. Due to the presence of multiple sensors embedded in the model, the excavation required extra caution and took approximately 5 to 7 days to complete.

The excavated sand from the first model was stored in its original location to the north of the Fears Lab. Soil excavated from the second model was stored in sealed buckets and later reused in the third model. After deconstructing the third model, both its soil and any remaining material from the second model were stored in sealed buckets inside the Fears Lab for potential future use.

Additionally, the geotextile and facing timbers were reused. Before reusing, the timber elements were cleaned and re-treated with waterproofing material. All geotextile-to-timber connections were inspected, and any loose staples were resecured to ensure structural integrity for subsequent model construction.

5. Model Instrumentation

Following the instrumentation plan reported by Esmaili et al. (2014), this study incorporated multiple sensors to monitor key parameters, including gravimetric water content, applied load, model deformation, and geotextile strain. The details of each measurement system are described in the following sections.

5.1 Moisture Sensors

After reviewing existing literature and evaluating practical applications, EC5 sensors were selected to monitor the gravimetric water content (GWC) of the model GRS bridge abutment backfill. These sensors provide continuous, real-time measurements of volumetric water content (VWC), which can be converted to GWC using the following relationship:

$$\theta = \mathrm{WC} \times \frac{\rho_d}{\rho_w} \tag{5.1}$$

Where:

θ = Volumetric water content (VWC) (m^3/m^3)

WC = Gravimetric water content (GWC) (%)

ρ_d = Dry density of soil (g/cm^3)

ρ_w = Density of water (g/cm^3)

The EC5 sensors were strategically positioned near the facing and at the soil–reinforcement interface to monitor variations in GWC within these critical zones of the abutment models (Figure 5.1). This placement enabled accurate tracking of moisture changes throughout all testing phases—before loading, during loading, and after failure. To ensure data reliability, all EC5 sensors were individually calibrated prior to each test.

Figure 5.1 Placement of EC5 sensors before the next lift

5.2 Linear Variable Differential Transformers (LVDT) and Wire Potentiometers (WP)

"SENSOTEC MDLC-1000" Linear Variable Differential Transformers (LVDTs), with a stroke length of 35 mm, were used to measure the settlement of the strip footing in the model GRS bridge abutment (Figure 5.2). Additionally, Celesco PT101 cable-extension position transducers (wire potentiometers) were used to monitor geotextile displacement. Thus, the obtained displacement is then used to calculate the strain in geotextile using strain equals change in length of geotextile over the original length of geotextile. The position of WPs was determined according to the log spiral curve (Chen and Snitbhan, 1975) for the failure surface (Figure 5.3). These high-precision sensors have a measurement range of 0 to 8 inches (≈203 mm) with an accuracy of 0.1% of full scale. The wire potentiometers were also attached to the model facing to track facing displacement during the loading phase. All LVDTs and wire potentiometers were calibrated prior to Model 1 and subsequently cross-checked before each model test to ensure measurement accuracy.

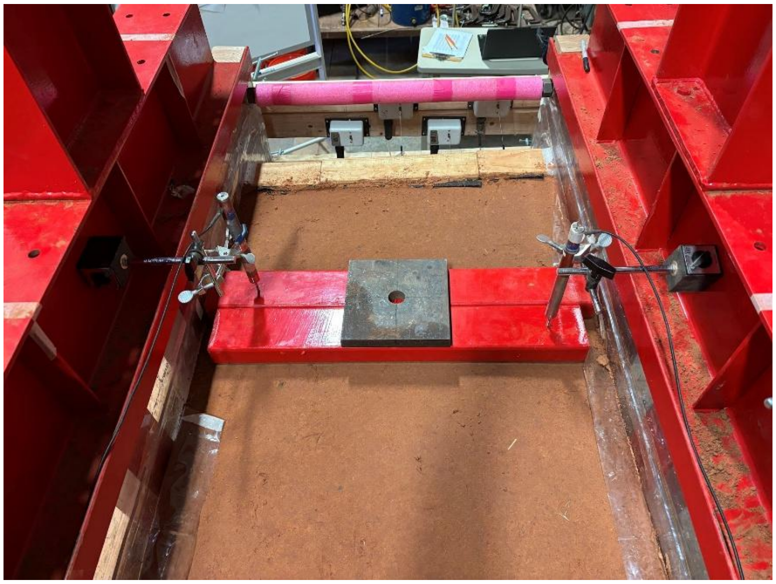

Figure 5.2 LVDTs were used to measure strip footing settlement

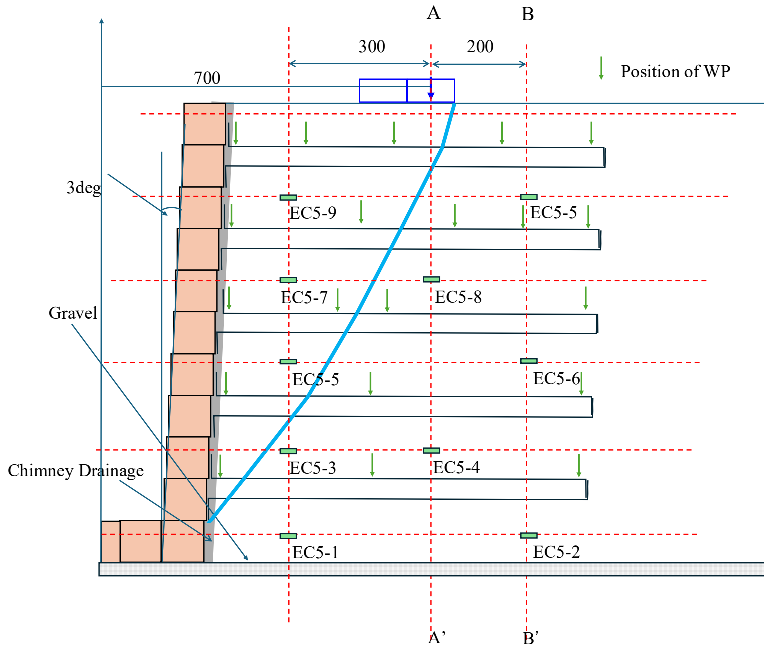

Figure 5.3 General layout of instrumentation based on log-spiral curve. Note: The light blue curve represents a theoretical log-spiral failure surface

5.3 Load cell

A compact “Interface 1232 AF-100K-B” load cell, of diameter 200 mm and height 115 mm, weighing 23.6 kg and capable of measuring loads up to 100 kips (≈ 450 kN), was used to monitor the applied vertical load on the model abutment (Figures 5.4 and 5.5). The load cell was positioned at the center of the strip footing to capture the load distribution accurately. Before testing Model 1, the load cell was calibrated, and its accuracy was reverified before the start of Models 2 and 3.

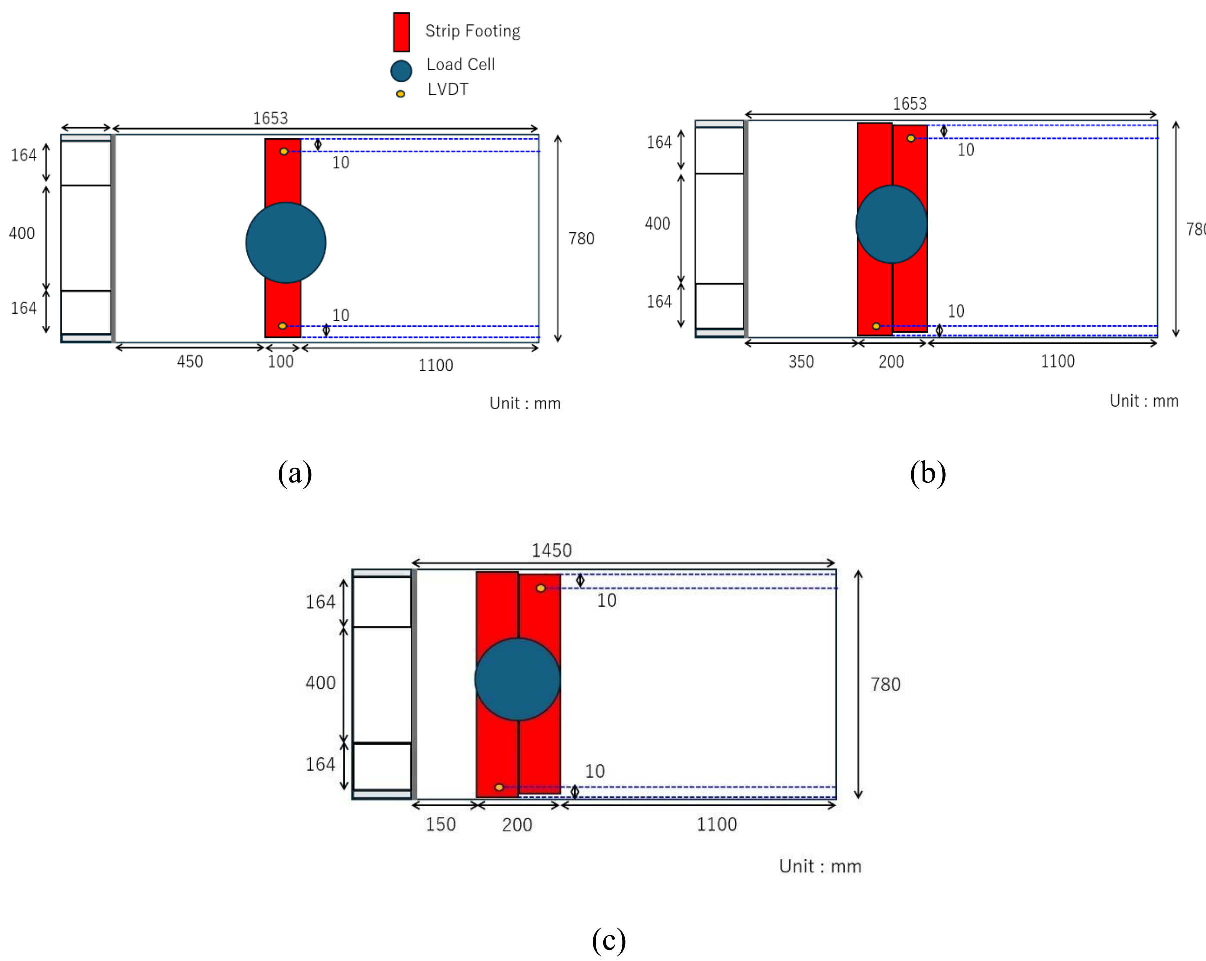

Figure 5.4 Top view of model abutments showing the locations of the footing, load cell, and LVDTs: (a) Model 1 – Phase 1, (b) Model 1 – Remaining Phases and Model 2, and (c) Model 3. The locations and dimensions of sensors are not shown to scale

Figure 5.5 Load cell used in the model tests

5.4 Instrumentation Plan

A total of 20 wire potentiometers (WPs) were used to measure displacement within the geotextile reinforcement layers, and 8 WPs were allocated for monitoring abutment facing movement in the first model (Figures 5.6 and 5.7). These 20 geotextile WPs were attached at the center of the three-partitioned top closely spaced geotextile layer, as illustrated in Figure 5.7. For Models 2 and 3, an additional 2 WPs were added to monitor the abutment facing, bringing the total to 30 WPs, as shown in Figures 5.6b and 5.6c.

In addition to the displacement sensors, 10 EC5 sensors were installed to monitor volumetric water content throughout the model backfill (Figure 5.6). Two LVDTs were used to record settlement of the strip footing (Figures 5.5 and 5.6), while a centrally placed load cell was used to measure the applied load on the model abutment (Figure 5.4). The complete instrumentation layouts for all model abutments are presented in Figures 5.4 through 5.7.

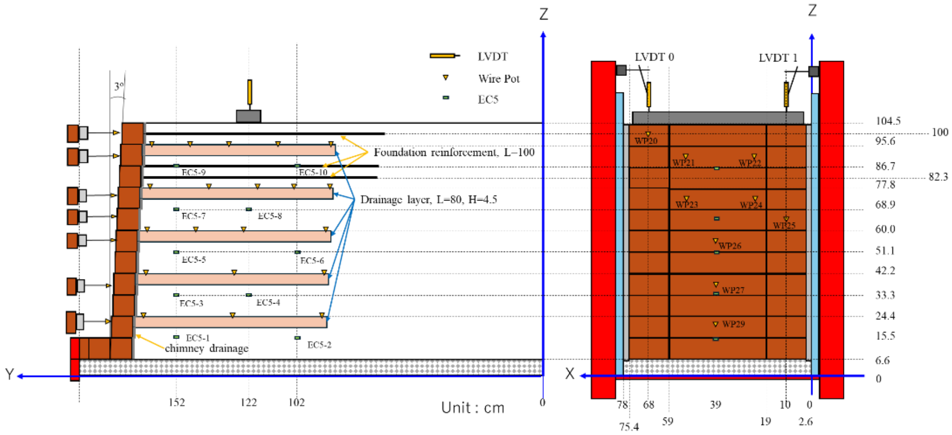

(a)

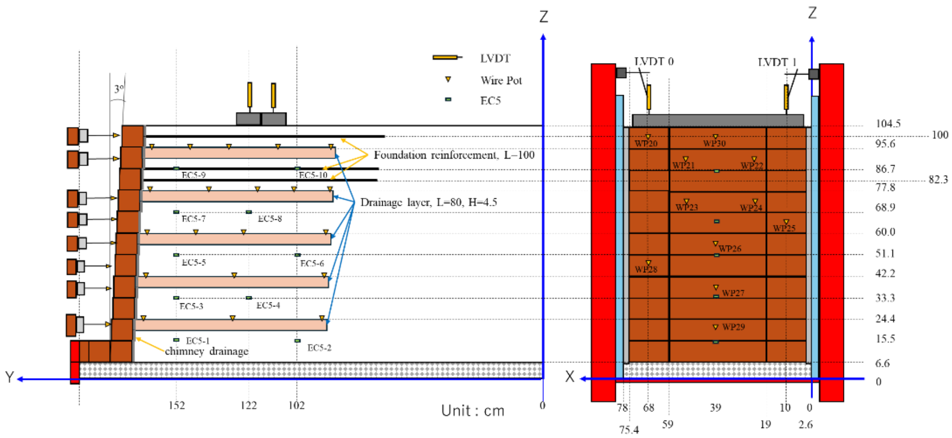

(b)

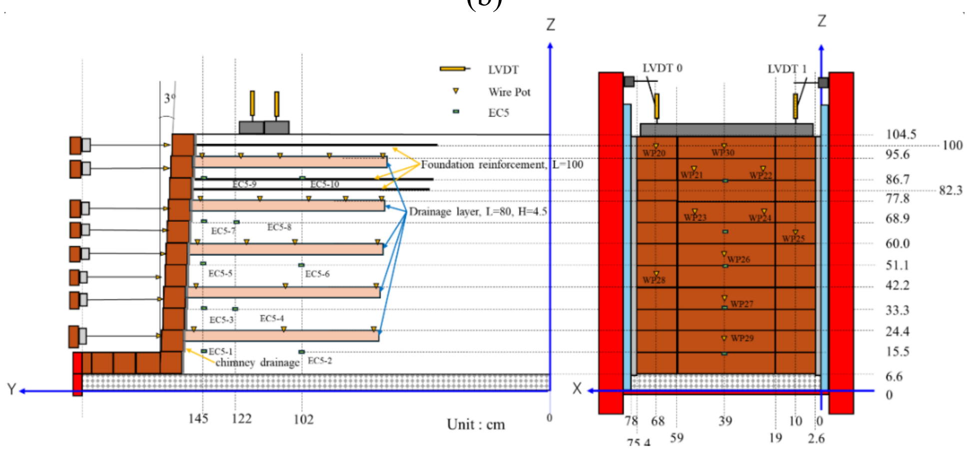

(c)

Figure 5.6 Instrumentation layout for the model GRS bridge abutments (side view and front view): (a) Model 1 – Phase 1, (b) Model 1 – Remaining Phases and Model 2, and (c) Model 3. Note: Sensor locations and dimensions are not shown to scale

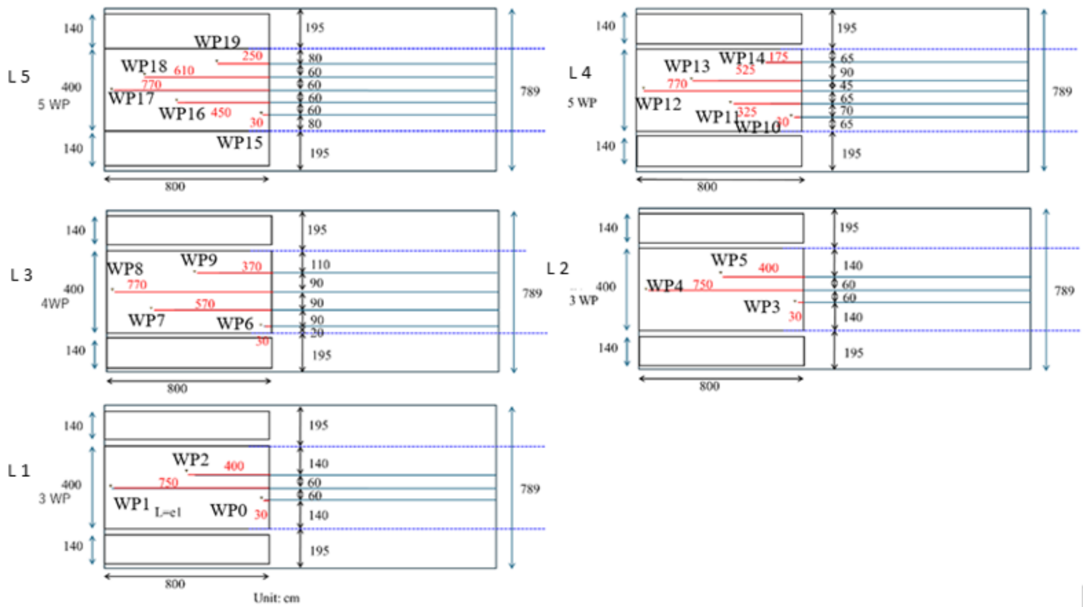

Figure 5.7 Plan view of the drainage layer reinforcement used in all model tests. Notes: (1) Sensor locations and dimensions are not shown to scale; (2) L1, L2,…L5 denote reinforcement layer numbers where L1 and L5 were located at the bottom and the top, respectively

The connection of wire potentiometers (WPs) to the geotextile layers for measuring internal displacement of the geotextile is shown in Figure 5.8. Figure 5.9 illustrates the placement of WPs on the rigid shelf located behind the test box.

Figure 5.8 Wire potentiometers (WPs) attached to the geotextile layer (L3)

Figure 5.9 Wire potentiometers (WPs) at the back of the test box

6. Results

6.1 Soil Water Content

6.1.1 During Construction

During the construction of the first model, the water content was measured using the microwave oven-drying method (ASTM D4643) for all model abutment facing layers, except for the bottom-facing panel layer and the 8th facing. Three soil samples were taken at distances of 100 mm, 390 mm, and 680 mm from the right side of the model at the location shown in Figure 6.1, immediately after soil compaction. Figure 6.2 shows the moisture distribution within the model during the construction phase. The measured moisture results are compared with the water content values obtained from the EC5 sensors after their placement to assess how closely the EC5 sensor readings match the measured water content values.

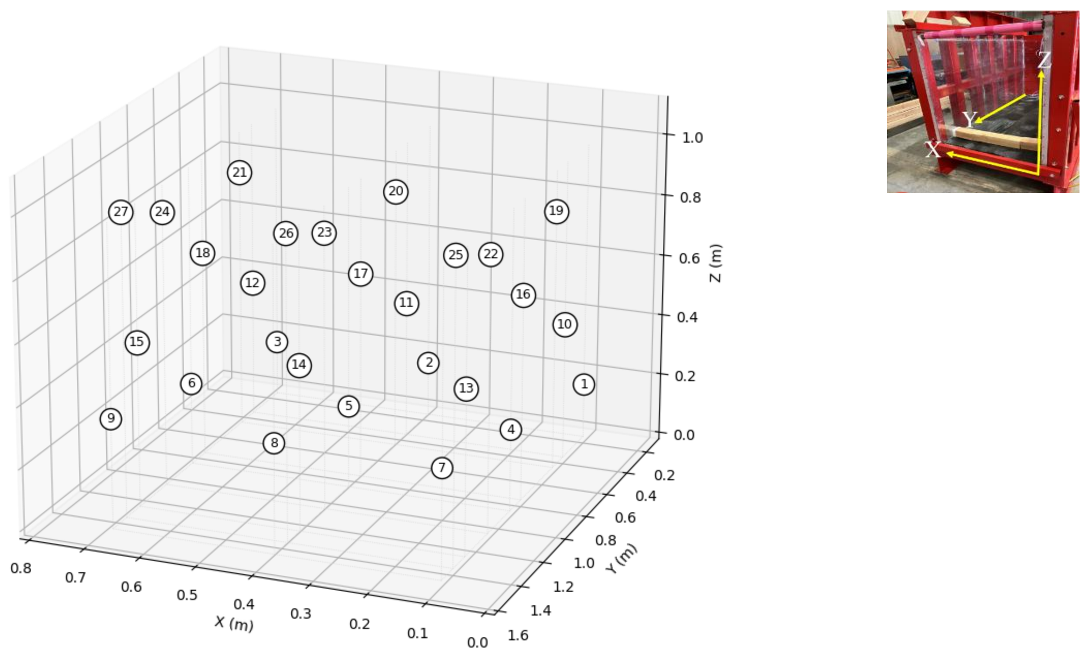

Figure 6.1 Sampling locations for water content measurements during the construction of Model 1.
Note: Numbered circles indicate the specific locations where samples were collected

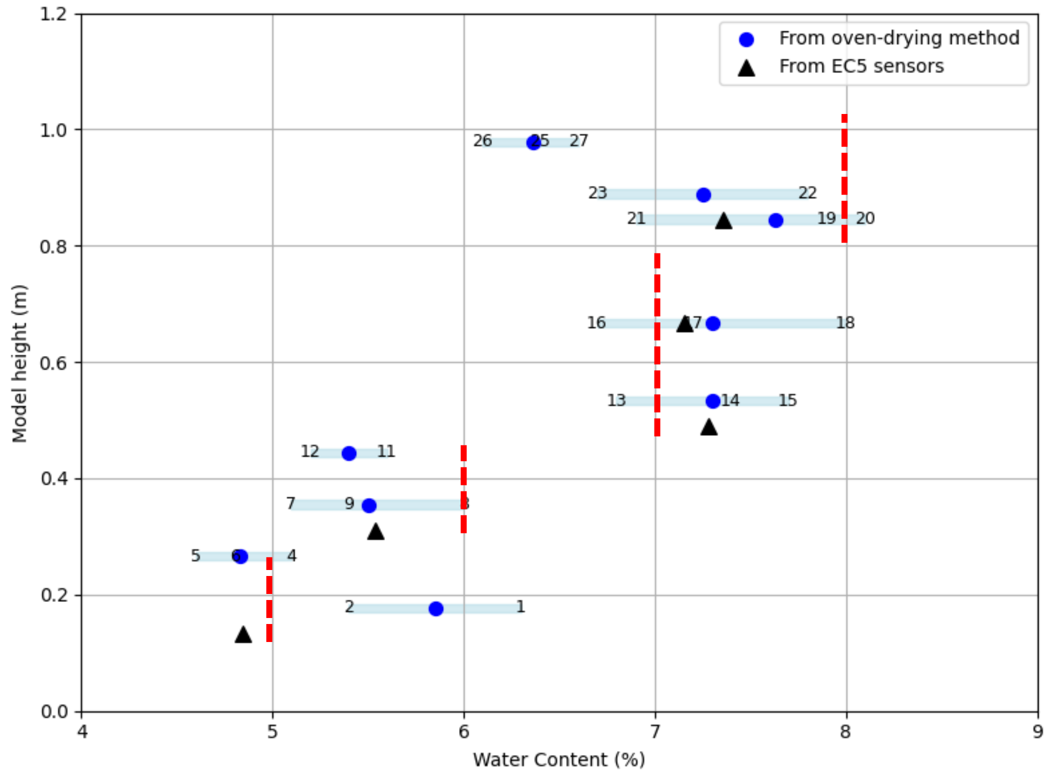

Figure 6.2 Water content distribution within the first model constructed using sand backfill, based on measurements obtained from oven-drying method and EC5 moisture sensors.
Notes: (1) The markers represent mean values from each method (2) The vertical red dashed line indicates the target water content, (3) the horizontal color band represents the range between the maximum and minimum measured water content values, (4) the numerical markers correspond to the measured values at specific locations in Figure 6.1

Based on the results from the first model, greater care was taken during the construction of the remaining two model abutments. For each lift, three soil samples were taken at locations shown in Figure 6.3 after compaction to determine water content using the microwave oven-drying method. Figure 6.4 shows the distribution of water content within the model abutment. Similar to Model 1, the measured water content values were compared with those obtained from the EC5 sensors after their placement.

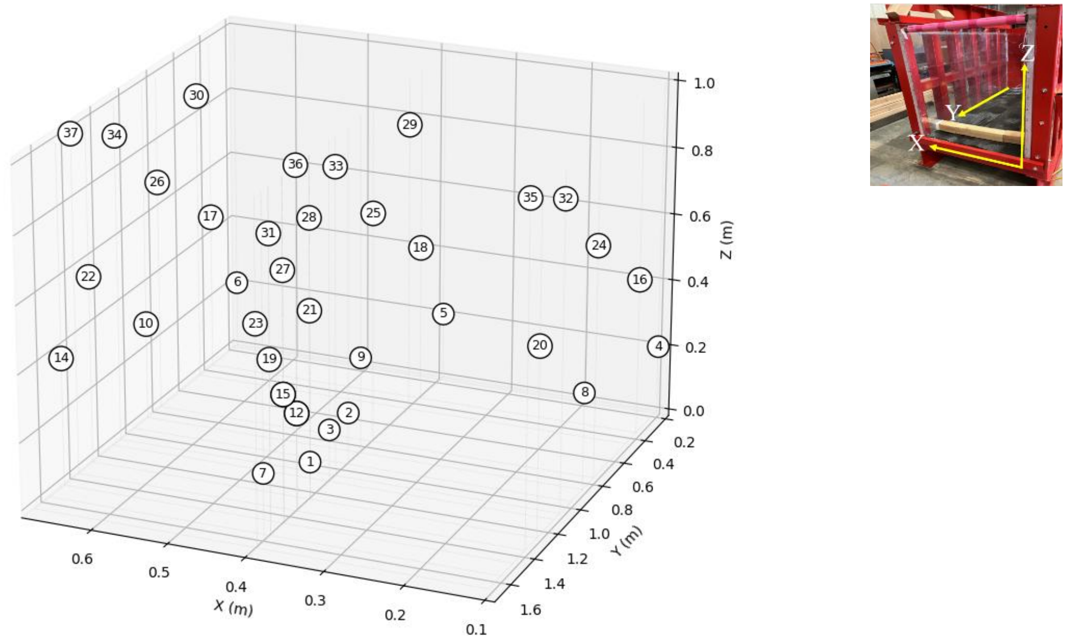

(a)

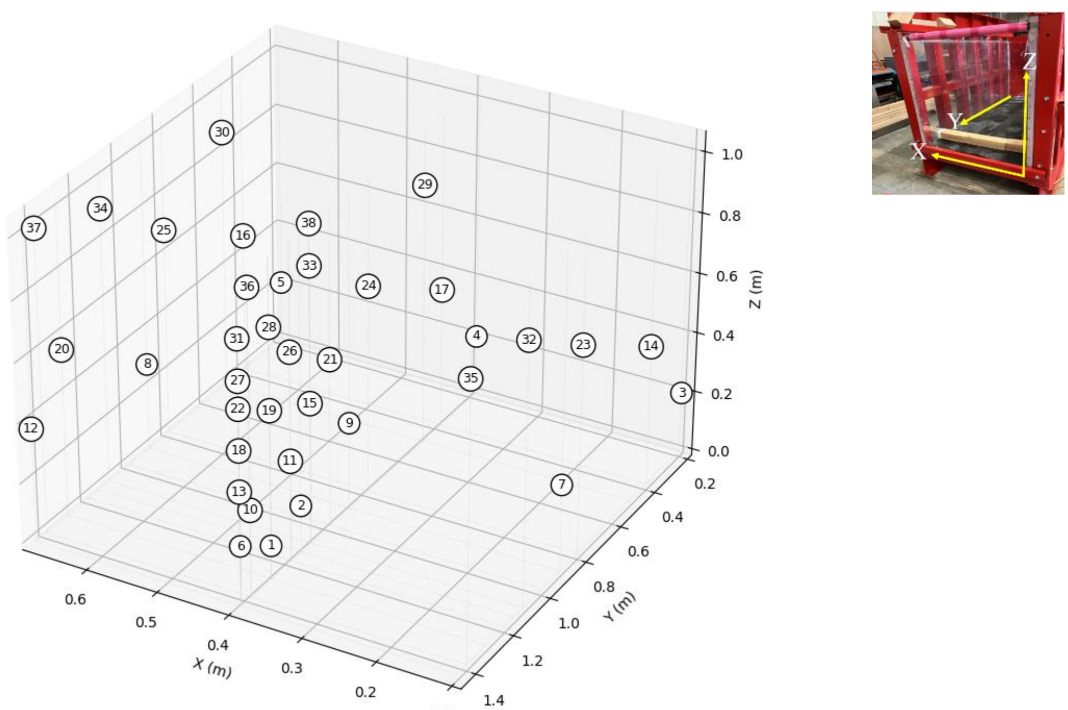

(b)

Figure 6.3 Sampling location for the water content during the construction of model abutments, (a) Model 2 (Marginal soil backfill), (b) Model 3 (Marginal soil backfill with footing placed near the facing). Note: Numbered circles indicate the specific locations where samples were collected

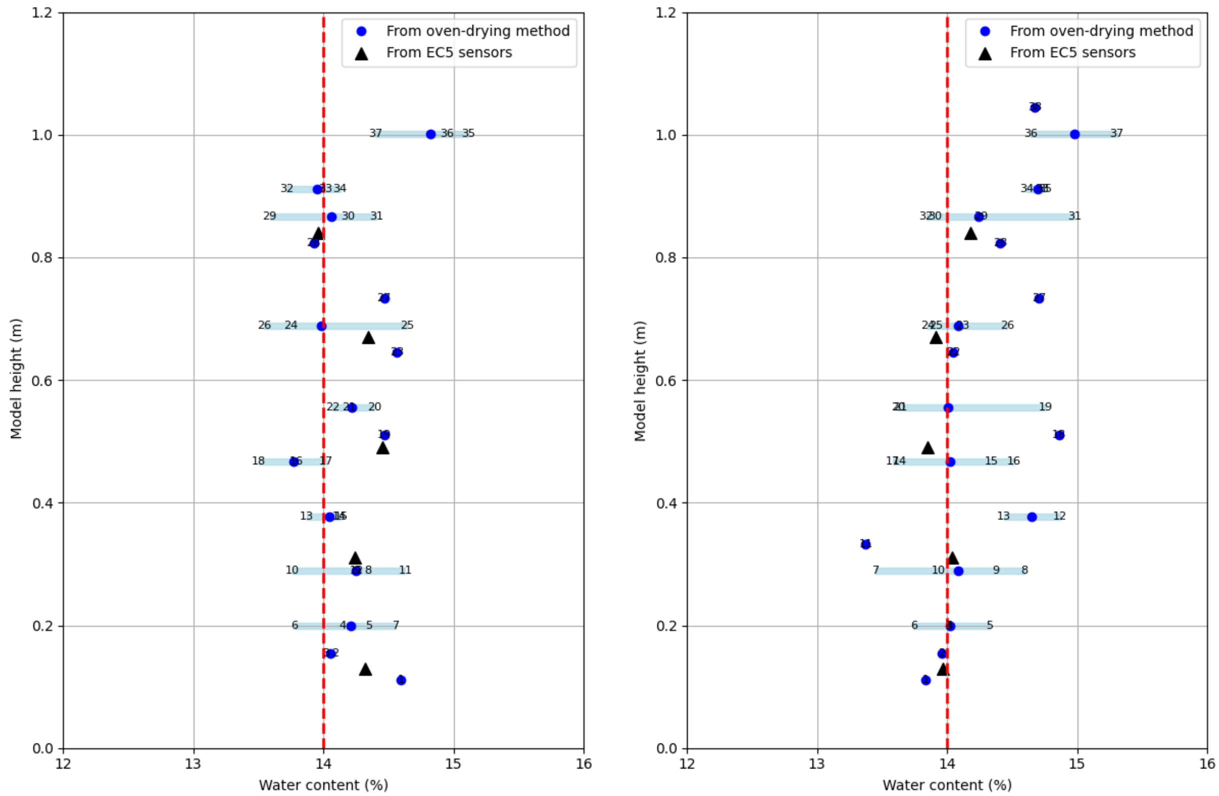

(a) (b)

Figure 6.4 Water content distribution within the model abutment, based on measurements obtained from oven-drying and EC5 moisture sensors, (a) Model 2, (c) Model 3.
Notes: (1) The markers represent mean values from each method (2) The vertical red dashed line indicates the target water content (OMC+3% = 14%), (3) the horizontal color band represents the range between the maximum and minimum recorded water content values, (4) the numerical markers correspond to the measured values at specific locations, as referenced in the location plot

The EC5 sensors were also used to monitor the water content of the soil within the model before and after testing. These sensors helped assess moisture stabilization before the start of the loading test. Figure 6.5 shows the water content variation with time, indicating that the model stabilized before each test phase.

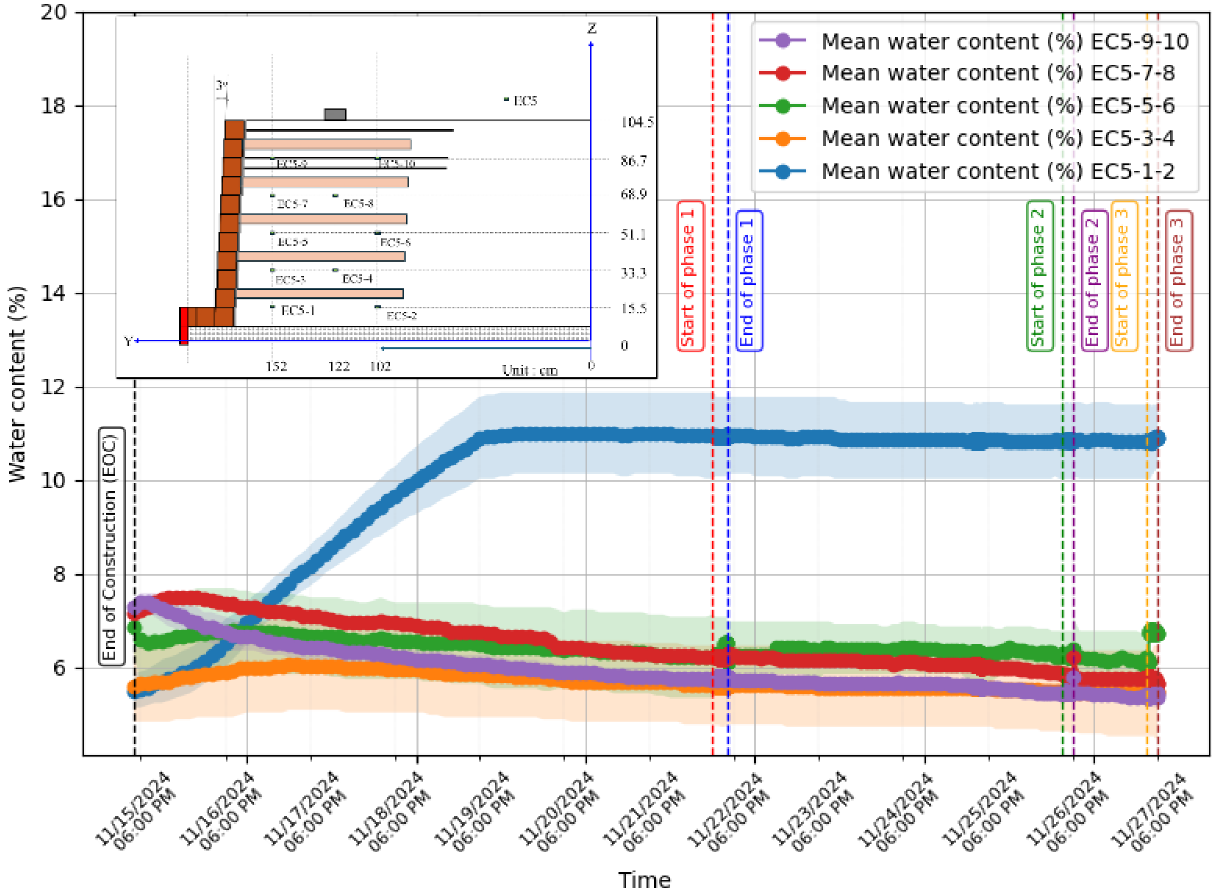

20
18
16
14
12
10
8
6
Water content (%)
Z
3°
EC5
104.5
86.7
68.9
51.1
33.3
15.5
0
Y
152
122
102
0
Unit : cm
EC5-9
EC5-10
EC5-7
EC5-8
EC5-5
EC5-6
EC5-3
EC5-4
EC5-1
EC5-2
Mean water content (%) EC5-9-10
Mean water content (%) EC5-7-8
Mean water content (%) EC5-5-6
Mean water content (%) EC5-3-4
Mean water content (%) EC5-1-2
End of Construction (EOC)
Start of phase 1
End of phase 1
Start of phase 2
End of phase 2
Start of phase 3
End of phase 3
11/15/2024 06:00 PM
11/16/2024 06:00 PM
11/17/2024 06:00 PM
11/18/2024 06:00 PM
11/19/2024 06:00 PM
11/20/2024 06:00 PM
11/21/2024 06:00 PM
11/22/2024 06:00 PM
11/23/2024 06:00 PM
11/24/2024 06:00 PM
11/25/2024 06:00 PM
11/26/2024 06:00 PM
11/27/2024 06:00 PM
Time

(a)

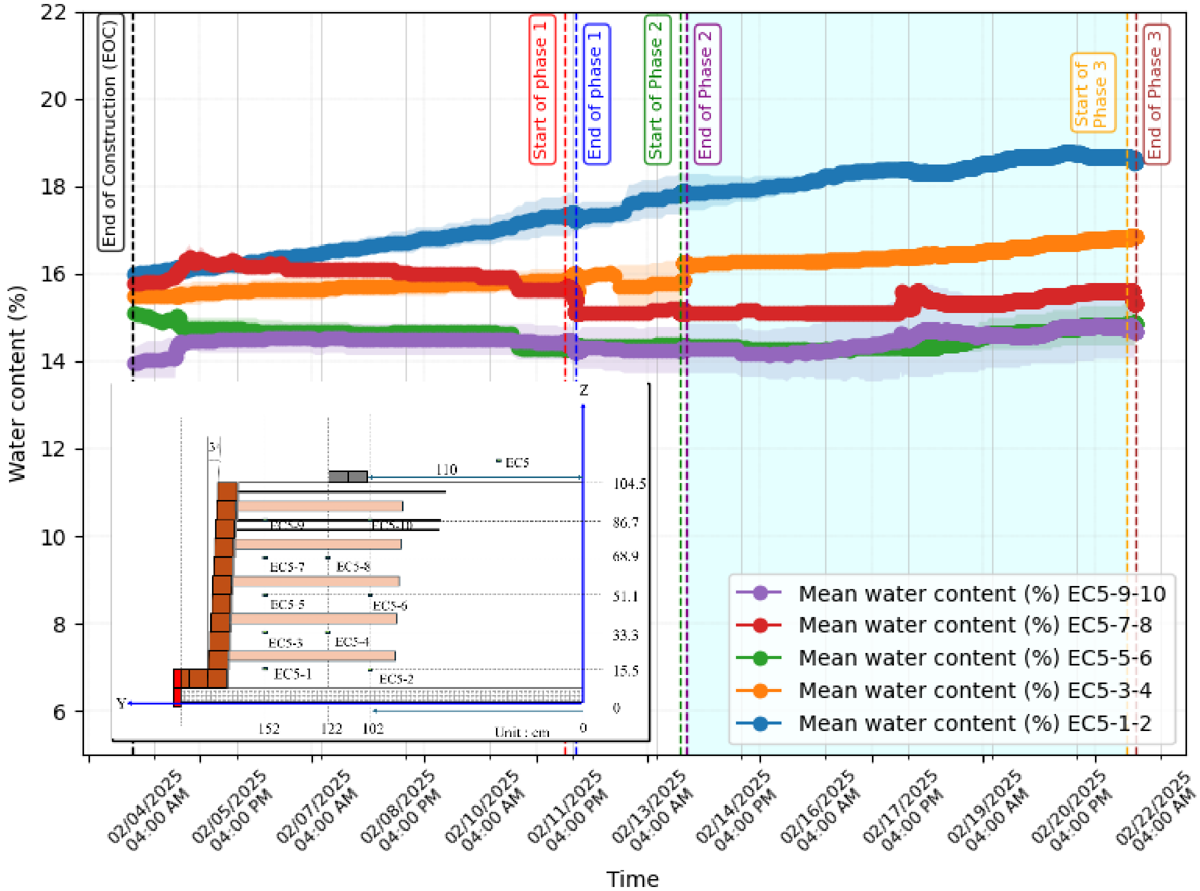

End of Construction (EOC)
Start of phase 1
End of phase 1
Start of Phase 2
End of Phase 2
Start of Phase 3
End of Phase 3
Water content (%)
Time
Mean water content (%) EC5-9-10
Mean water content (%) EC5-7-8
Mean water content (%) EC5-5-6
Mean water content (%) EC5-3-4
Mean water content (%) EC5-1-2
Unit : cm

(b)

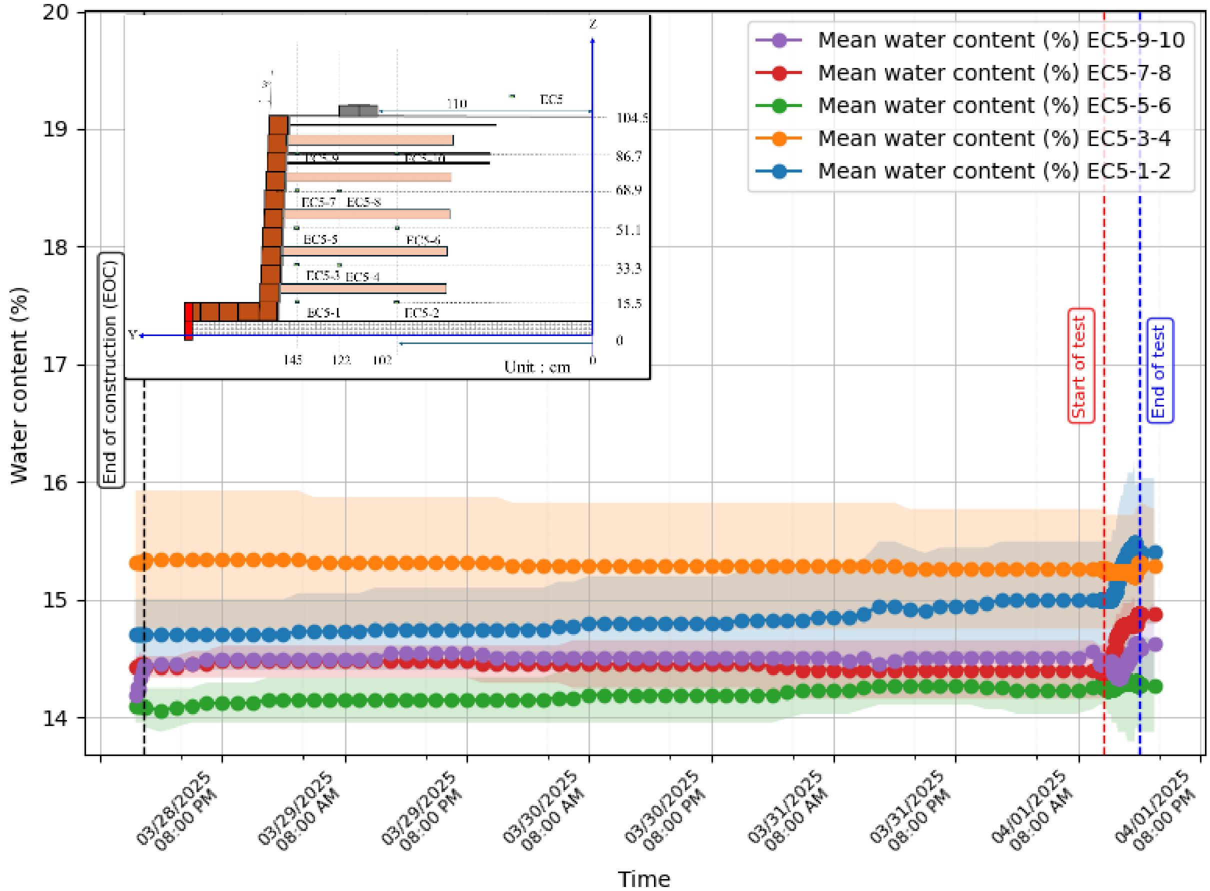

(c)

Figure 6.5 Average water content from EC5 sensors: (a) Model with sand backfill, (b) Model with marginal soil backfill, (c) Model with marginal soil backfill and footing placed near the facing. Notes: (1) The vertical dashed lines indicate the loading phases of model abutments, (2) The band represents the range between the maximum and minimum water content values recorded by each pair of EC5 sensors, where the lower edge of the band corresponds to the minimum value and the upper edge corresponds to the maximum value

6.1.2 Wetting of Backfill

For the second model abutment, the loading phase was also conducted following an attempt to increase the water content in the backfill. In addition to recording the water collected in the bottom drainage tub, EC5 sensors were utilized to monitor the internal moisture distribution within the model. Figure 6.5b illustrates the moisture profile during this phase, confirming that moisture equilibrium was achieved prior to the onset of loading. The aqua-colored vertical band in Figure 6.5b denotes the wetting period. However, the figure also shows that the water content did not increase significantly, and full saturation was not achieved. As a result, the data from this phase were not analyzed in the present study but are included here as supplementary information for future reference.

6.1.3 During Deconstruction

During the deconstruction process of the second and third model abutments, the water content distribution within the models was also measured. Three samples per lift were taken at the location shown in Figure 6.6 to check the compaction degree; the water content was determined from these samples using the microwave oven-drying method, except for the lifts containing drainage layers (Figure 6.7).

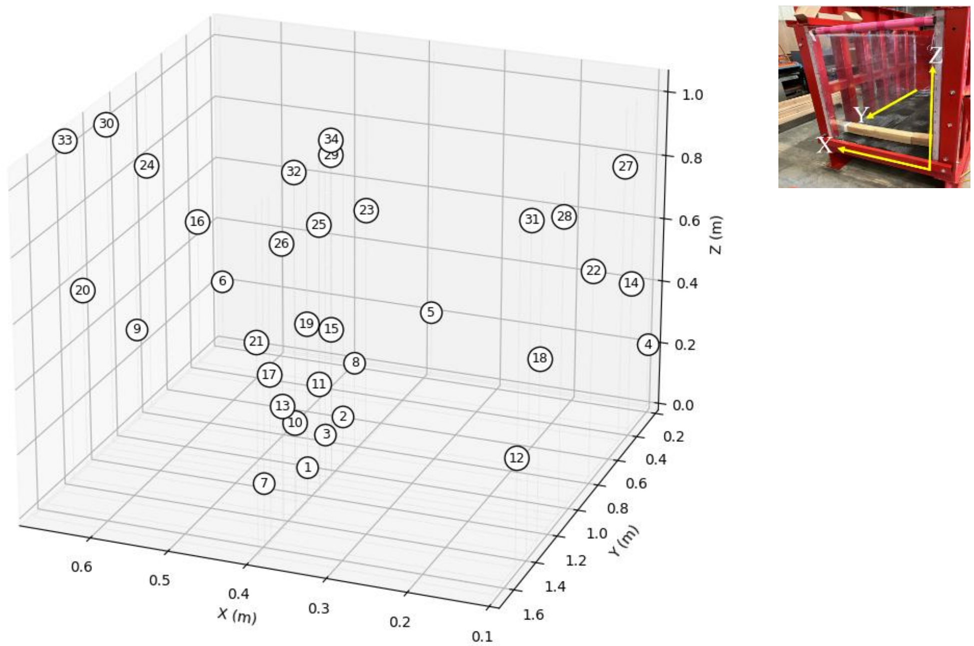

(a)

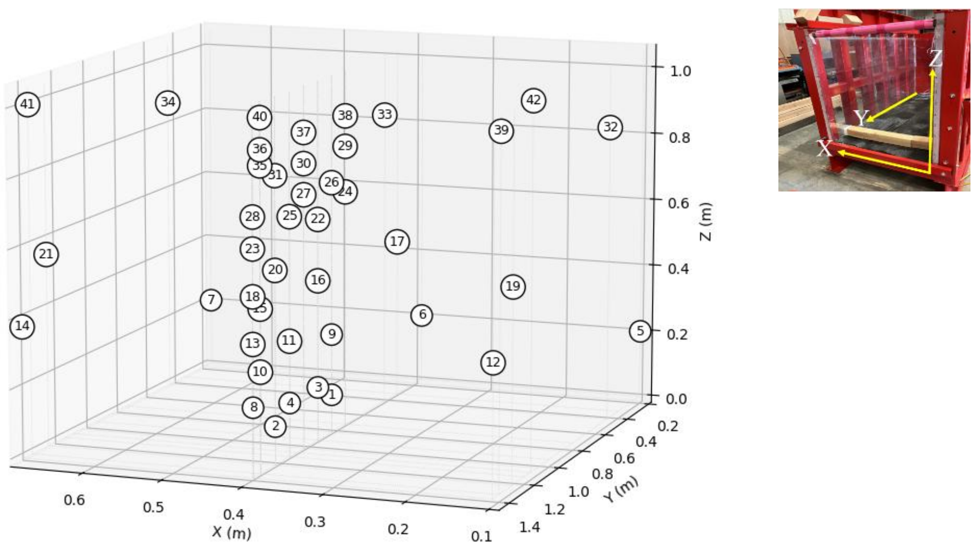

(b)

Figure 6.6 Sampling location during the deconstruction of model abutments, (a) Model 2 (Marginal soil backfill), (b) Model 3 (Marginal soil backfill with footing placed near the facing).
Note: Numbered circles indicate the specific locations where samples were collected.

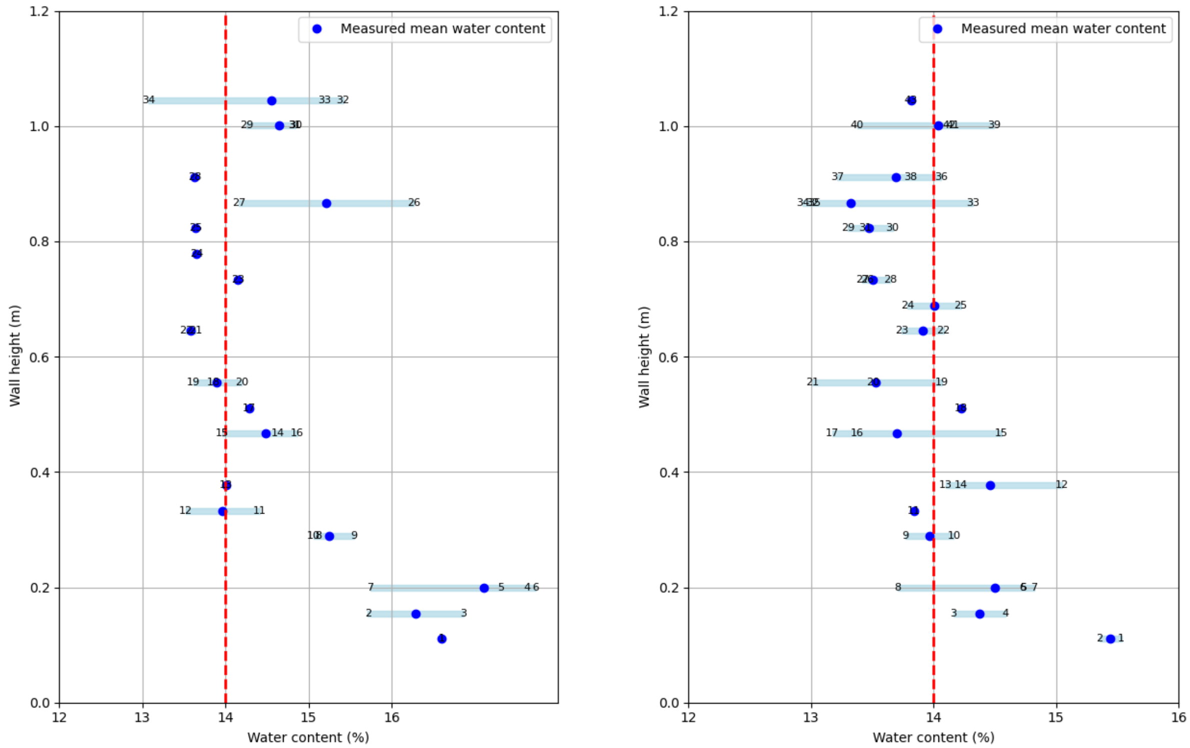

(a) (b)

Figure 6.7 Water content distribution during the deconstruction within the model abutments, based on data from the oven-drying method (a) Model 2, (b) Model 3.
Notes: (1) The vertical red dashed line indicates the target water content, (2) the horizontal color band represents the range between the maximum and minimum recorded water content values, (3) the numerical markers correspond to the measured values at specific locations, as referenced in the location plot

6.2 Dry Unit Weight and Degree of Compaction

For the second and third model abutments, the compaction degree and dry unit weight were also monitored during both the construction and deconstruction stages. Samples were taken at the locations specified in Figure 6.6, except for the lifts containing drainage layers. These samples were also used for water content determination. Figure 6.8 shows the distribution of dry unit weight and compaction degree within the model abutments.

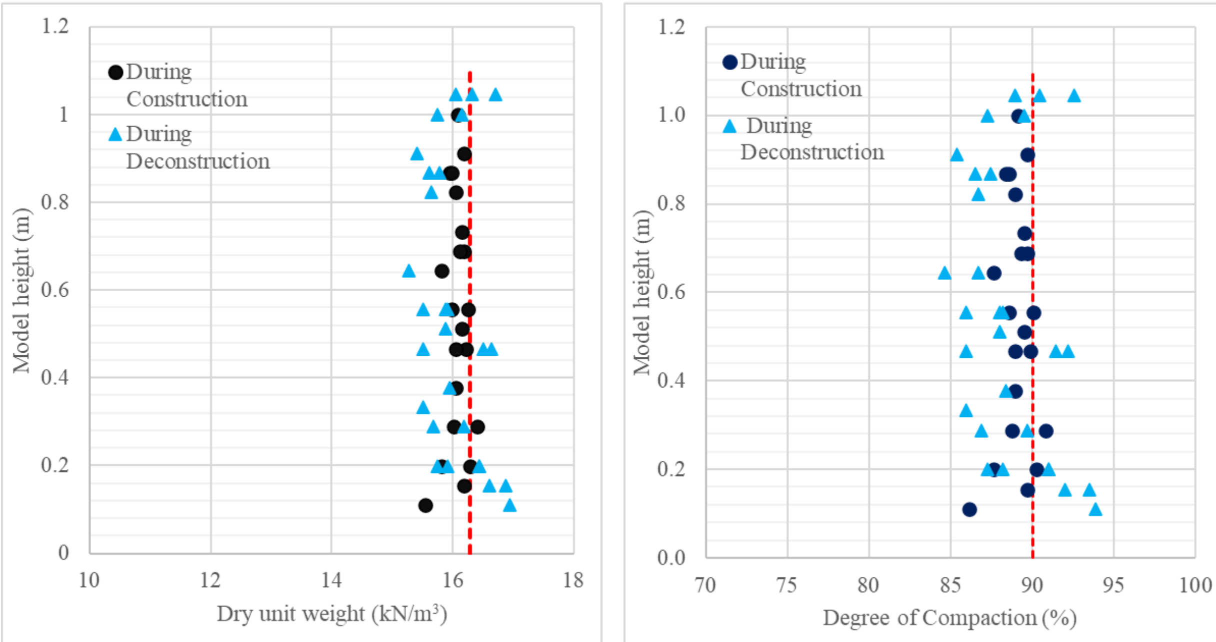

(a)

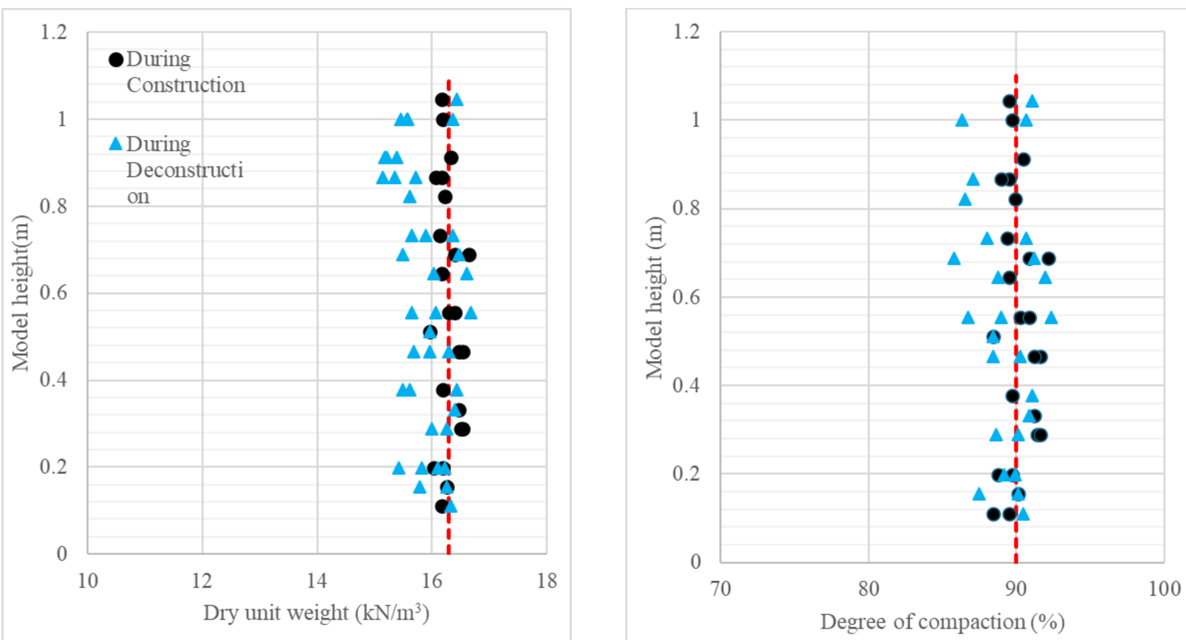

(b)

Figure 6.8 Dry unit weight and degree of compaction during construction within the model abutments using marginal soil as backfill. (a) Second model, (b) Third model with footing placed near the facing. Note: The vertical red dashed line represents the target dry unit weight and compaction degree

6.3 Load Settlement Data

Table 6.1 shows the summary data obtained in this study for all the model abutments tested.

Table 6.1 Summary data for model abutments tested in this study

Model	Load			Mean Footing Displacement at (mm)		Maximum Facing Displacement at (mm)		Reinforcement Strain at (%)		
	Load for 0.5% H settlement (kPa)	Final (kPa)	Final (kips)	Service Load (190 kPa)	Final Load	Service Load (190 kPa)	Final Load	Service Load (190 kPa)	Final Load	Layer
1 (Sand backfill)	254	1,418	6.7	3.9	27.3	1	9.6	0.2	1.68	L4
2 (Marginal soil backfill with water content OMC +3%)	250.2	1,800	59.36	4.6	23.7	1.1	9.8	0.3	2.35	L4
2 (Marginal soil backfill with an attempt to increase the water content)	261.5	2,122	70.07	4.4	21.6	0.2	5.3	0.1	1.45	L5
3 (Footing placed near to the facing	201.4	2,038	67.21	4.9	43.9	1.1	16.7	0.48	3.01	L3

Note: The maximum difference in footing settlement recorded between the two sensors was 1.1 mm for Model 1, 2.2 mm for Model 2 (OMC + 3%), 2.8 mm for Model 2 (wet backfill), and 3.7 mm for Model 3.

Figure 6.9 shows the load-settlement response of all three model abutments, including the multistage loading sequence conducted on Model 2. The applied vertical load is plotted against the measured settlement of the strip footing. The FHWA design criteria for bridge abutments with a service load of 190 kPa (4,000 lb/ft^2) and a limiting settlement of 0.5% of the abutment height (i.e., 0.5%H = 5.23 mm) are also indicated in the figure for reference.

All model abutments were subjected to load levels beyond the service load until a crack was observed. However, due to safety concerns, including hydraulic jack malfunction caused by oil leakage, and the test box not being wide enough, the tests were terminated after reaching their final load values. Visual signs of structural damage, such as surface cracks, were recorded at the time of test termination and are shown in Figure 6.11. The full load-settlement behavior up to final loads are presented in Figure 6.10, and the corresponding final load values are summarized in Table 6.1.

At the service load, Model 1 (sand backfill, control case) exhibited the smallest settlement, confirming its superior stiffness. In contrast, Model 3 (marginal soil backfill with load applied near the facing) showed the largest settlement, approximately 26% higher than Model 1. Model 2, constructed with marginal soil at 14% water content, exhibited 18% more settlement, while the saturated condition of Model 2 showed a 13% increase compared to the control model. Despite these differences, all models remained within the FHWA's allowable settlement limit of 0.5% H, with actual settlements being 6%, 12%, and 25% below the threshold for Models 3, 2 (OMC+3%), and Model 1 (control case), respectively.

These results confirm that the model abutment constructed with sand backfill exhibited the highest stiffness, while the model with loading near the facing demonstrated the lowest. Nonetheless, all models met the performance criteria for serviceability, with measured settlements remaining below the FHWA-specified limit under the 190 kPa service load. The performance of marginal soil models was also acceptable, confirming their potential use in geosynthetic reinforced bridge abutment applications when appropriately reinforced.

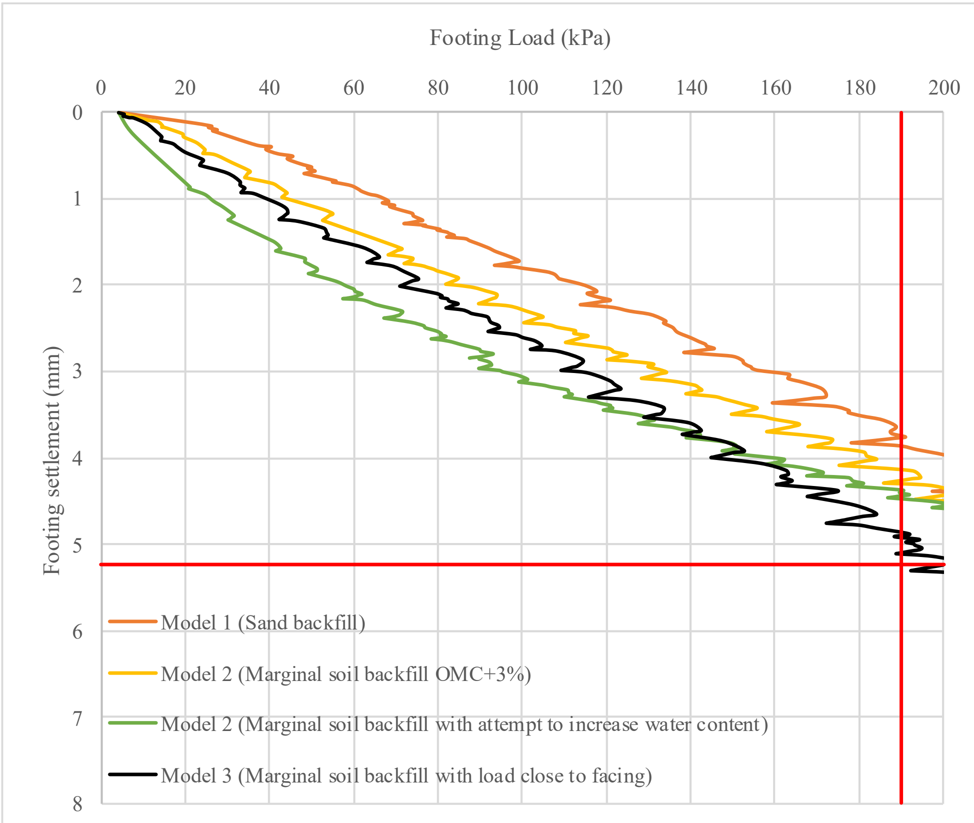

Figure 6.9 Load-settlement data for all the model abutments. Notes: (1) For all model abutments, the load-settlement behavior was first observed at service load, as per FHWA guidelines; (2) the vertical solid red line represents the service load (4,000 lb/ft^2 ≈ 190 kPa); and (3) the horizontal solid red line indicates the limiting settlement, defined as 0.5% of the model height

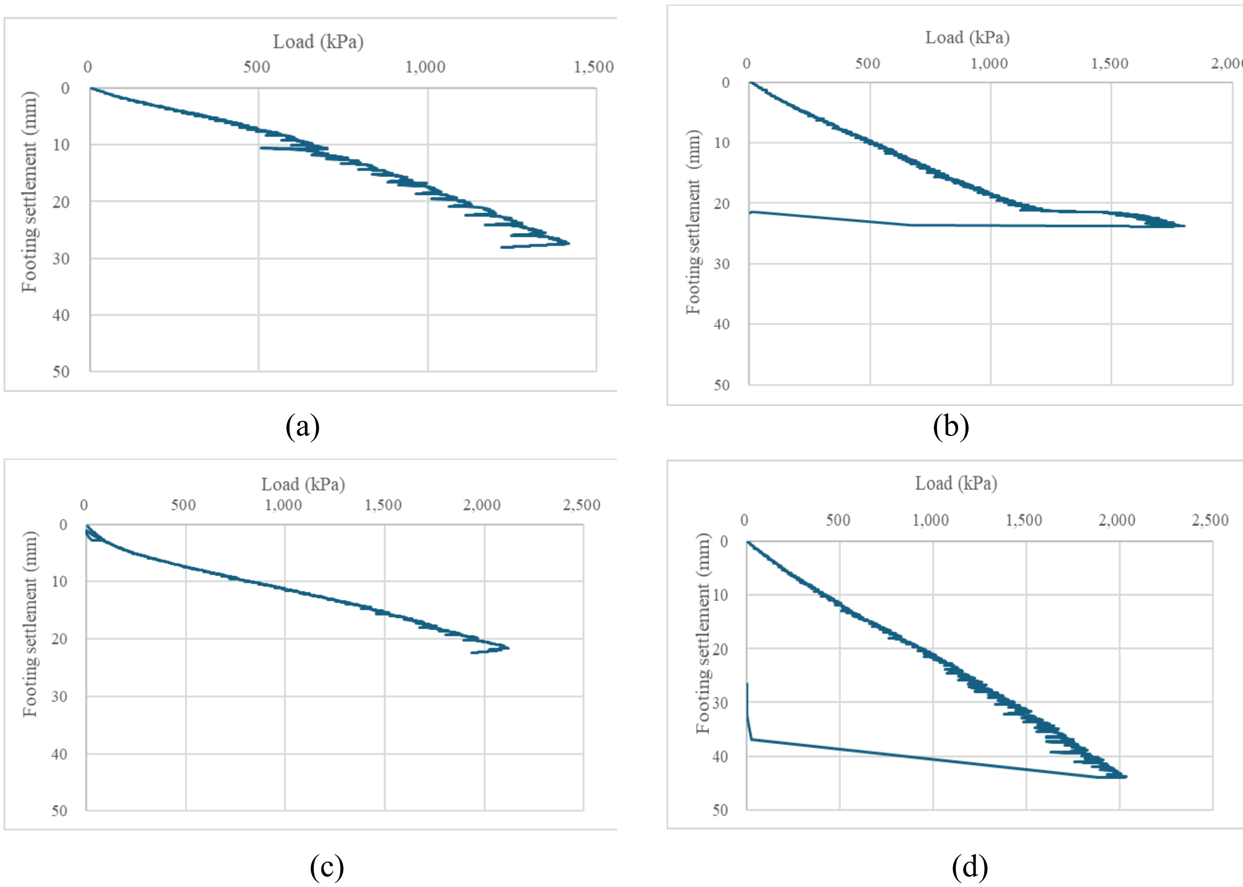

Figure 6.10 Load-settlement response of the model abutments. (a) First model constructed with sand backfill, (b) second model constructed with marginal soil backfill with 14% water content, (c) second model with marginal soil backfill under wet conditions, and (d) third model with marginal soil backfill subjected to loading near the facing

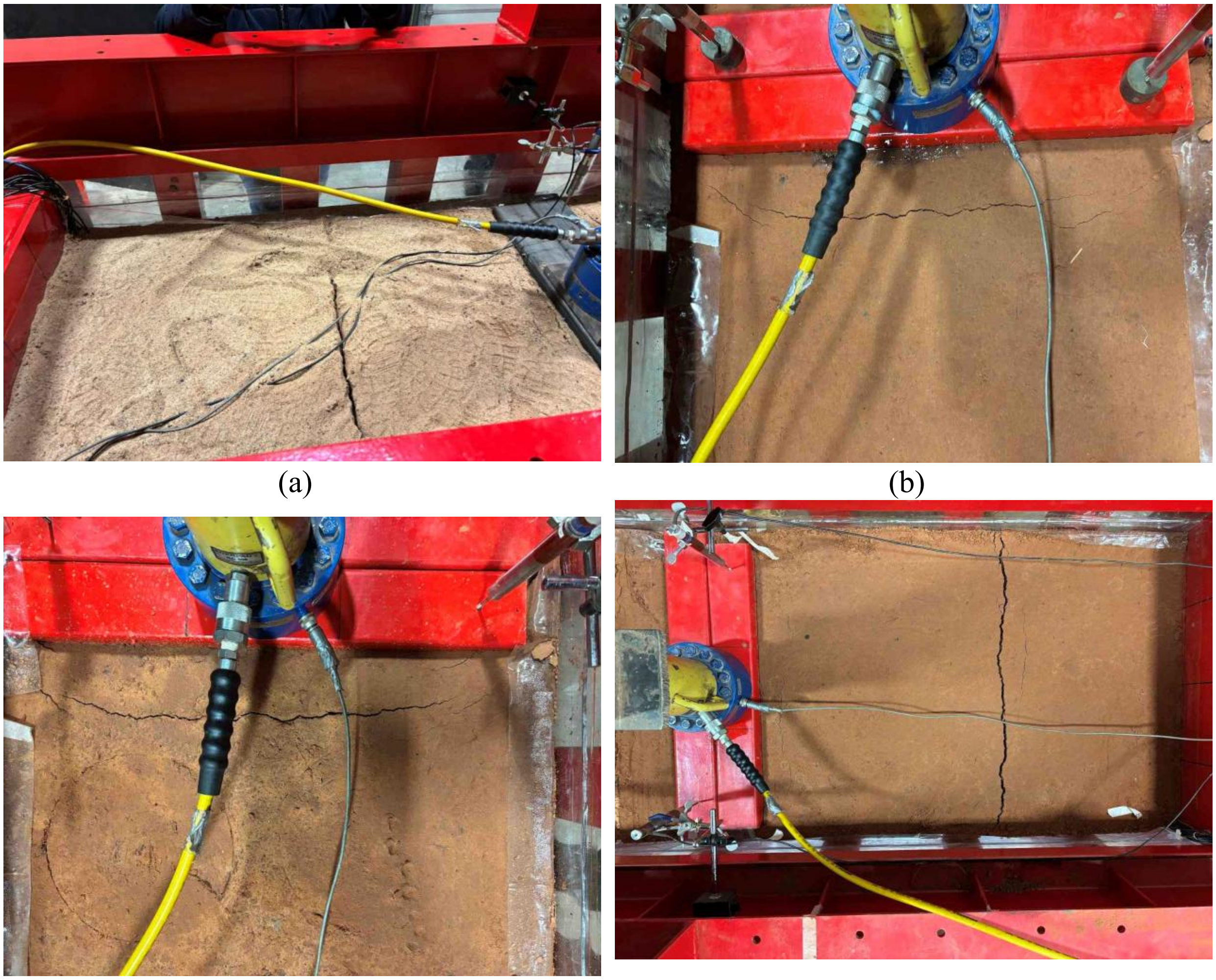

(a) (b) (c) (d)

Figure 6.11 Structural damage observed in the model abutments at the point of test termination: (a) First model constructed with sand backfill, (b) second model with marginal soil backfill at 14% water content, (c) second model with marginal soil backfill under wet condition, and (d) third model with marginal soil backfill subjected to loading near the facing

6.4 Facing Displacements

Facing displacements were measured using wire potentiometers installed on the facing blocks, as shown in Figure 5.5 of the instrumentation section. However, for this study, only the wire potentiometer readings from the center wooden block were used to analyze the lateral displacement of the model. Figure 6.12a compares the facing displacements of all model abutments under the allowable service load. All measured displacements were significantly below the FHWA-specified lateral displacement limit of δ_{max} = 1%H = 10.45 mm, where H represents the abutment height (FHWA 2018).

The maximum lateral displacements recorded were 1.0 mm, 1.1 mm, and 1.1 mm for Model 1 (sand backfill), Model 2 (marginal soil backfill at OMC + 3%), and Model 3 (marginal soil backfill with loading applied near the facing), respectively. These correspond to normalized displacements of δ/H = 0.096%, 0.105%, and 0.105%. For Model 2 (marginal soil backfill with an attempt to increase moisture content), the maximum lateral facing displacement was only 0.2 mm (δ/H = 0.019%).

Consistent with FHWA guidelines for bridge abutments, the greatest lateral displacements were observed in the upper third of the abutment height. Overall, the results show that all model abutments remained within the serviceability limits, including those constructed with marginal soil backfill (OMC + 3%), and subjected to loading near the facing (150 mm from the back of the facing). These findings demonstrate the potential for using marginal soil as backfill in this type of GRS abutment design.

Figure 6.12b presents a comparison of the maximum lateral facing displacements of all model abutments when subjected to their final loading conditions. Although these data were not used in the present analysis, they are included here as supplementary information for potential future reference.

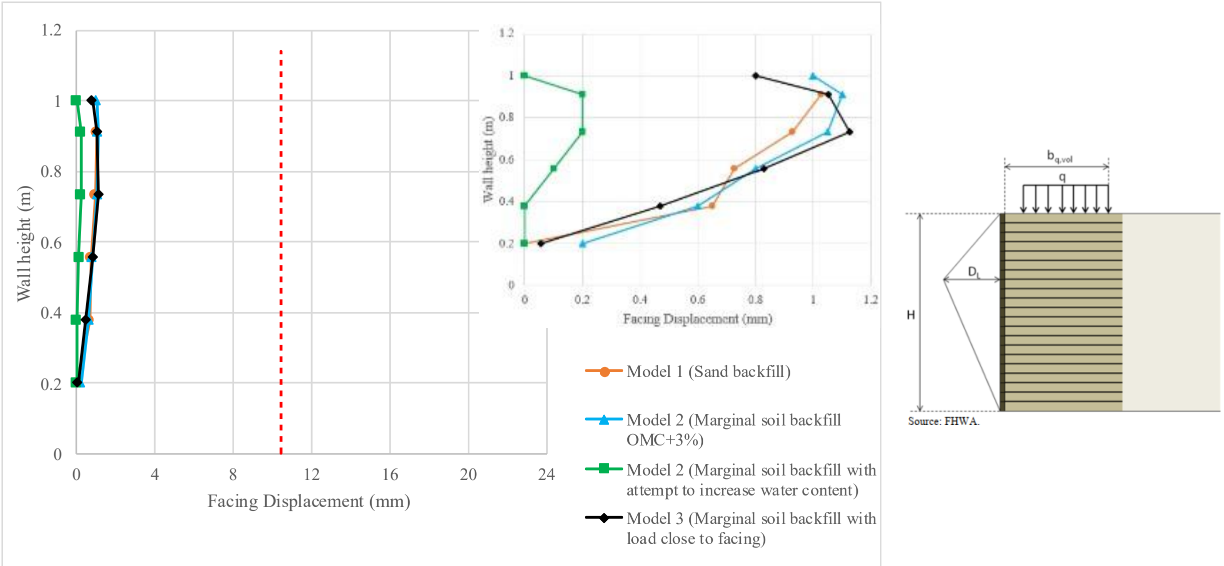

(a)

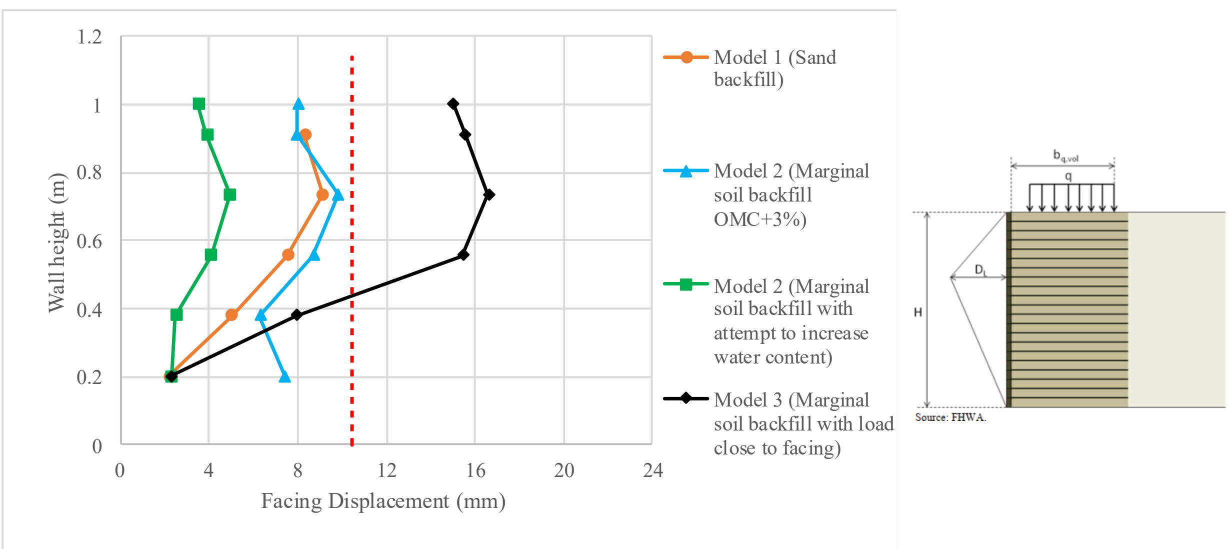

(b)

Figure 6.12 Facing displacement along the height of all model abutments: (a) Displacement recorded under the allowable service load, including a zoomed-in view, (b) displacement profile along the model height when subjected to final load. Notes: (1)The red vertical dashed line indicates the allowable facing displacement limit of 10.45 mm as per FHWA guidelines, (2) Figure on the right shows the maximum lateral deformation occurs in the top third of the abutment per FHWA (2018)

6.5 Reinforcement Strains

Figure 6.13 presents the maximum geosynthetic strain profiles along the abutment height for all model tests. The results closely align with the facing displacement data, with the highest strain values observed in the upper third of the abutment consistent with expected deformation behavior.

Figure 6.14 shows the strain distribution within the geotextile layers positioned at the top of the closely spaced reinforcement zones under the allowable service load of 190 kPa. All measured strain values were well below the FHWA-specified limiting strain of ε_{max} = 2% (FHWA 2018). The figure also indicates that the highest strain values occurred near the loading location, denoted by the green band. The maximum strain values observed were 0.20%, 0.30%, and 0.48% for Model 1 (sand backfill), Model 2 (marginal soil backfill at OMC + 3%), and Model 3 (marginal soil backfill with loading applied near the facing), respectively. In Model 2, with an attempt to increase moisture content, the maximum strain was only 0.06.

Figure 6.15 illustrates the strain distribution under the final loading conditions for all model walls. As noted earlier, these data are not part of the primary analysis but are included as supplementary information for future reference.

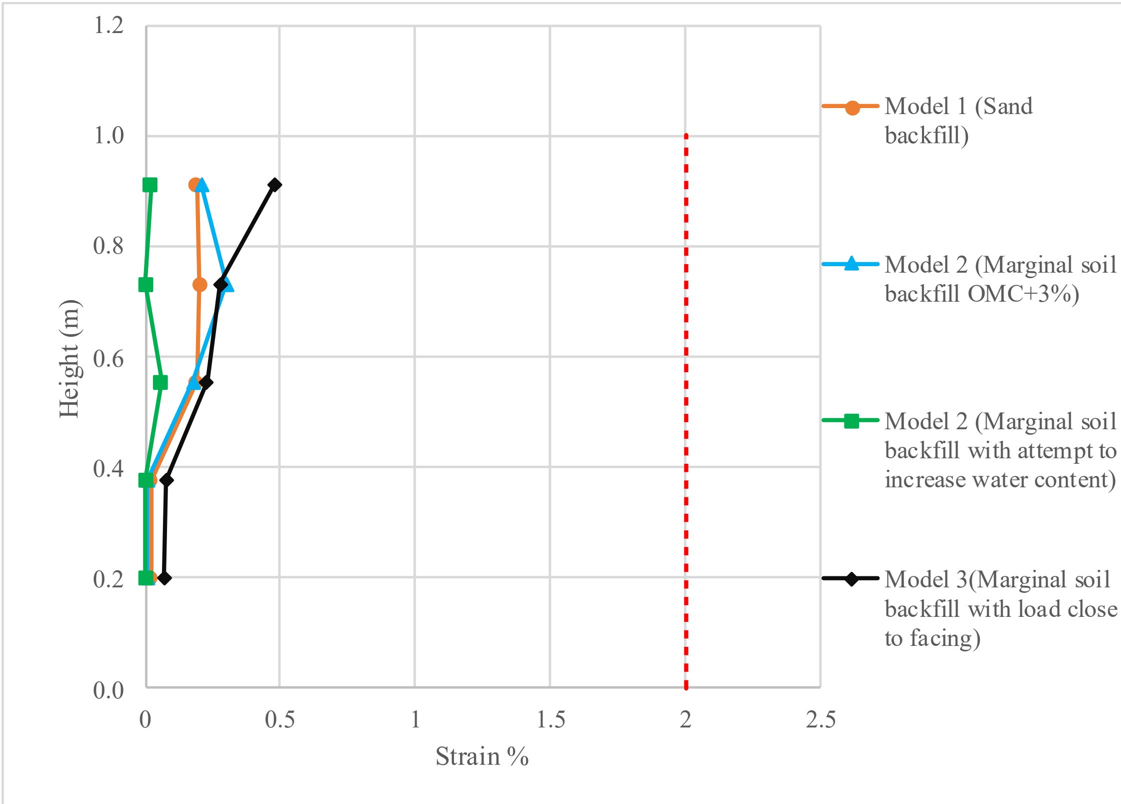

Figure 6.13 Profile of maximum geosynthetic strain along the abutment height. Note: The red vertical dashed line indicates the limiting geotextile strain of 2% as per FHWA guidelines

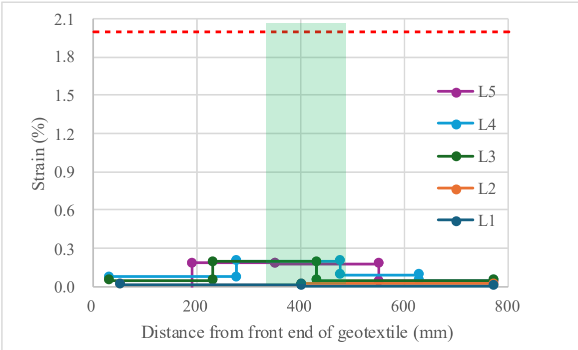

(a)

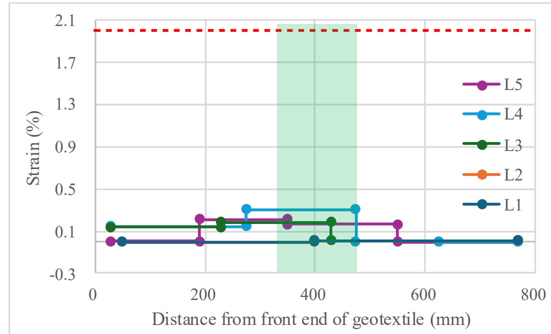

(b)

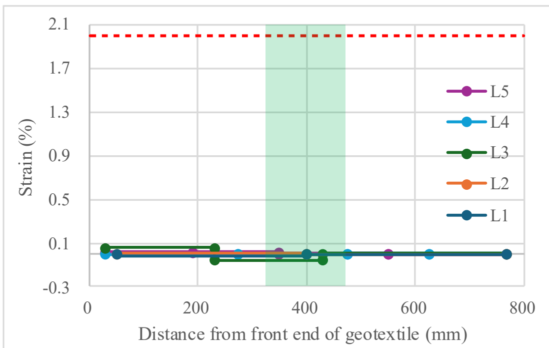

(c)

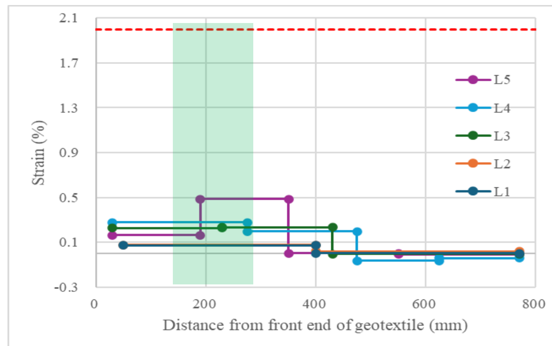

(d)

Figure 6.14 Strain distribution within the geotextile layers positioned at the top of the closely spaced reinforcement zones for all model abutments under the allowable service load: (a) Model 1, (b) Model 2, (c) Model 2 with attempt to increase the moisture condition, and (d) Model 3. Notes: (1)The horizontal red dashed line represents the limiting strain of 2% as per FHWA guidelines, (2) The green vertical band represents the footing location

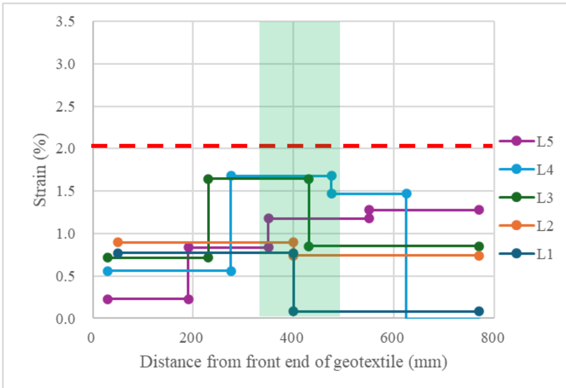

(a)

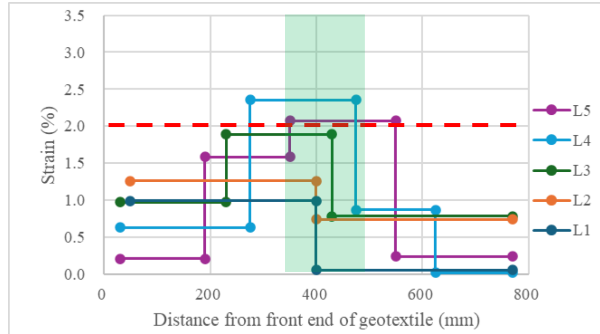

(b)

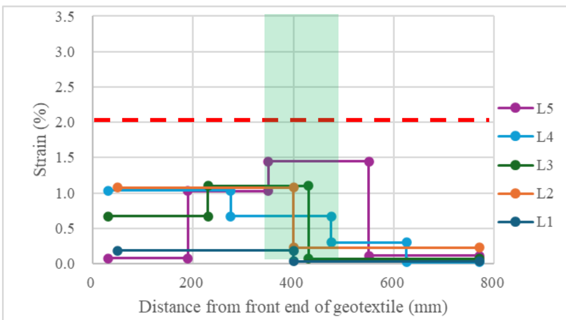

(c)

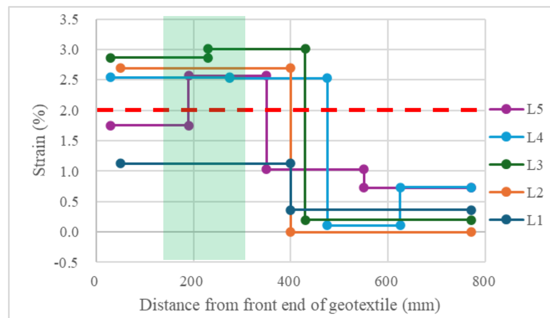

(d)

Figure 6.15 Strain distribution within the geotextile layers positioned at the top of the closely spaced reinforcement zones for all model abutments under the final load: (a) Model 1, (b) Model 2, (c) Model 2 with attempt to increase the moisture condition, and (d) Model 3. Notes: (1)The horizontal red dashed line represents the limiting strain of 2% as per FHWA guidelines, (2) The green vertical band represents the footing location

7. Conclusions and Recommendations

7.1 Conclusions

Three specially designed model GRS bridge abutments were constructed within a test box and load-tested to evaluate the design performance using marginal soil as a potential backfill material, and to assess how such fill affects load-bearing capacity. Each model had a nominal height of 1.05 m and was constructed using the same geometric design. The models were instrumented to monitor facing deformations, load-settlement behavior at the abutment top surface, reinforcement strains, and moisture distribution within the backfill.

The control model was backfilled with clean sand that met FHWA specifications (fines content < 12%, i.e., 0.5%, and Plasticity Index ≤ 6, i.e., 0). In contrast, the other two models were backfilled with marginal soil, which exceeded FHWA limits (fines content = 24.7%) and PI =0. All models featured a unique design with closely spaced reinforcement layers.

The results of the study indicate the following:

1. Load Capacity and Deformation Compliance: All three model GRS bridge abutments successfully carried the FHWA-recommended service load of 190 kPa while remaining within the allowable settlement, facing deformation, and reinforcement strain limits.
2. Comparative Performance: The control model with sand backfill exhibited the stiffest response. However, both Model 2 (marginal soil backfill compacted at OMC + 3%) and Model 3 (marginal soil backfill compacted at OMC + 3% and loaded near the facing) also remained within allowable limits, highlighting the potential for marginal soils to be used effectively in GRS abutment designs.

3. Strain and Lateral Displacement Limits: Reinforcement strains and maximum lateral facing displacements in all three models were significantly below the FHWA allowable limits of 2% and 1% H (H=abutment height), respectively, when subjected to the 190 kPa service load. These observations further support the suitability of marginal soils as backfill in properly reinforced GRS systems.
4. Setback Validation for Marginal Soils: For Model 3, in which the load was applied near the facing (setback of 15 cm), all recorded load-settlement, strain, and facing displacement values remained within FHWA limits under the service load. Applying a scale factor of 2 to this finding suggests that a setback of 30 cm (approximately 12 inches) would be adequate for full-scale abutments. This aligns well with the FHWA recommendation of maintaining a setback greater than 8 inches, thereby validating the design.

7.2 Observations

During the testing of the model abutments, several practical observations were made that, while not directly part of the analytical scope of this study, are important and may provide useful insights for future research and experimental work. These observations include, but are not limited to, the following:

1. The model abutments investigated in this study, even though were built at a reduced scale, were sufficiently large to include field-scale materials and they were also tested under field-scale load magnitudes. If a scaling factor is to be considered, it should be interpreted as a range rather than a fixed value. According to FHWA guidelines for GRS bridge abutments using open-graded aggregates, the maximum grain size recommended for optimal compaction ranges between 0.5–1.5 inches. By comparing the upper bound of

this range (1.5 inches) to the maximum grain size of the select backfill sand used in this study (0.37 inches), a scale factor of approximately 4 is obtained, although this is not necessarily the most appropriate basis for scaling, as sand is also commonly used in full scale abutments. Additionally, based on the reinforcement spacing of 12 inches recommended by FHWA and 5.3 inches used in this study, a scale factor of approximately 2.26 is derived. Therefore, the model abutments in this study can be considered to represent a scale range between 2.26 and 4.

2. The tests on Model 2 and Model 3 began with relatively conservative conditions of marginal soil compacted at OMC + 3% and a 90% degree of compaction. Despite these non-ideal parameters, both models met FHWA serviceability criteria. This suggests that, in field applications where backfill soil is compacted closer to optimum moisture content (OMC), similar or improved performance can reasonably be expected.

3. When testing the model abutments beyond the service load, it was observed that the structure withstood significantly higher loads. However, due to the confined dimensions of the test box, it is possible that the entire box system was mobilized at higher loads rather than just the model itself. This may have led to an overestimation of the load-bearing capacity in those phases. Future studies should consider larger test setups or additional boundary isolation to mitigate this issue.

4. In the third phase of testing Model 2, the abutment exhibited behavior consistent with that of a pre-stressed system, as it had already experienced loading in previous phases. As a result, minimal strain, settlement, and lateral deformation were observed during this phase. This highlights the importance of accounting for previous loading history when interpreting performance metrics in multi-phase testing scenarios.

7.3 Recommendations for Future Study

The work described in this thesis is a part of an ongoing study in that, the three model abutments constructed and tested in this phase are meant to serve as control for comparisons with future test cases. To expand the scope and deepen the understanding of the behavior of GRS bridge abutments with marginal soils, the following recommendations are made:

1. In this study, a specially engineered marginal soil with fines content greater than 12% and a Plasticity Index (PI) of 0 was used. Future tests should consider soils with fines greater than 12% and PI greater than 6 to evaluate the performance of abutments backfilled with higher-plasticity materials, further extending the study beyond current FHWA guidelines.
2. To investigate the influence of reinforcement properties on abutment behavior, future testing should include different types of geosynthetics, such as needle-punched geotextiles or woven fabrics, especially in combination with marginal soils.
3. In the third phase of Model 2, the attempt to increase water content was ineffective due to preferential flow paths along the back of the model abutment. Future studies should adopt improved saturation techniques, such as gradual infiltration or multiple injection points, to ensure uniform moisture distribution throughout the backfill.
4. This study utilized a closely spaced reinforcement layout. Future tests should explore the effects of modifying the spacing, such as removing top or bottom reinforcement layers or increasing spacing intervals, to assess the influence of reinforcement configuration on abutment performance with marginal soils.

5. The narrow width of the test box used in this study may have contributed to unintended boundary constraints, particularly under higher loading conditions. Future experimental setups should consider wider boxes or designs that minimize sidewall influence to better replicate field conditions.
6. In the current design, reinforcement layers were stapled to the facing, forming a semi-composite structure. To evaluate the role of the facing in load transfer, future tests could use the same model geometry and materials but with reinforcement layers not physically connected to the facing.
7. The marginal soil used in this study consisted of 15% clay and 85% silt, with an OMC of 11%, a friction angle of 38.8°, and cohesion of 7.1 kPa at OMC. To assess the influence of backfill strength on abutment performance, future models should incorporate weaker soils, such as a 40% clay and 60 % silty sand mix. Preliminary direct shear tests on such a mix at an OMC of 14.1% yielded a friction angle of 34.9° and cohesion of 9.8 kPa.
8. Due to time constraints, the long-term effects of moisture variation were not studied. Future research should include moisture conditioning (e.g., saturation) after abutment construction to simulate flooding or seasonal changes and examine their impact on abutment deformation and overall performance.

References

Abdi, M.R., and Mirzaeifar, H., 2017, “Experimental and PIV Evaluation of Grain Size and Distribution on Soil–Geogrid Interactions in Pullout Test.” *Soils and Foundations* 57 (6): 1045–1058. https://doi.org/10.1016/j.sandf.2017.08.030.

Abu-Farsakh, M. Y., Almohd, I., and Farrag, K., 2006, “Comparison of Field and Laboratory Pullout Tests on Geosynthetics in Marginal Soils.” *Transportation Research Record: Journal of the Transportation Research Board* 1975 (January):124–136. https://doi.org/10.1177/0361198106197500114.

Abu-Farsakh, M.Y., Ardah, A., and Voyiadjis, G.Z., 2019. “Numerical Parametric Study to Evaluate the Performance of a Geosynthetic Reinforced Soil–Integrated Bridge System (GRS-IBS) under Service Loading.” *Transportation Geotechnics* 20 (September):100238. https://doi.org/10.1016/j.trgeo.2019.04.001.

Adams, M., Nicks, J., 2018. “Design and Construction Guidelines for Geosynthetic Reinforced Soil Abutments and Integrated Bridge Systems." *FHWA Publication No: FHWA-HRT-17-080 HRDI-40/06 18(200)E*. Federal Highway Administration, Washington, D.C., USA.

ASTM International D698, 2021, “Standard Test Methods for Laboratory Compaction Characteristics of Soil Using Standard Effort (12,400 ft-lbf/ft3 (600 kN-m/m3))”, *American Society for Testing and Materials,* West Conshohochen, PA, USA.

ASTM International D854, 2023, “Standard Test Methods for Specific Gravity of Soil Solids by the Water Displacement Method”, *American Society for Testing and Materials,* West Conshohochen, PA, USA.

ASTM International D2487, 2006, “Standard Practice for Classification of Soils for Engineering Purposes (Unified Soil Classification System)”, *American Society for Testing and Materials,* West Conshohochen, PA, USA.

ASTM International D4318, 2018, “Standard Test Methods for Liquid Limit, Plastic Limit, and Plasticity Index of Soils”, *American Society for Testing and Materials,* West Conshohochen, PA, USA.

ASTM International D3080, 2023, “Standard Test Method for Direct Shear Test of Soils Under Consolidated Drained Conditions”, *American Society for Testing and Materials,* West Conshohochen, PA, USA.

ASTM International D4643, 2017, “Standard Test Method for Determination of Water Content of Soil and Rock by Microwave Oven Heating”, *American Society for Testing and Materials,* West Conshohochen, PA, USA.

ASTM International D6913, 2009, “Standard Test Methods for Particle-Size Distribution (Gradation) of Soils Using Sieve Analysis”, *American Society for Testing and Materials,* West Conshohochen, PA, USA.

Balakrishnan, S., and Viswanadham, B.V.S., 2016, “Performance Evaluation of Geogrid Reinforced Soil Walls with Marginal Backfills through Centrifuge Model Tests.” *Geotextiles and Geomembranes* 44 (1): 95–108. https://doi.org/10.1016/j.geotexmem.2015.06.002.

Berg R.B., Christopher, B.R. and Naresh C. Samtani, 2009, “Design and Construction of Mechanically Stabilized Earth Walls and Reinforced Soil Slopes”, *Federal Highway Administration, Washington, DC, USA, FHWA-NHI-10-024*.

Bui Van, D., Chinkulkijniwat, A., Horpibulsuk, S., Yubonchit, S., Limrat, I., Arulrajah, A., and Jothityangkoon, C., 2017, “Steady Flow in Mechanically Stabilised Earth Walls Using Marginal Soils with Geocomposites.” *Geosynthetics International* 24 (6): 590–606. https://doi.org/10.1680/jgein.17.00026.

Chen, W.F., and Snitbhan, N., 1975. “On Slip Surface and Slope Stability Analysis.” *Soils and Foundations* 15 (3): 1–15. https://doi.org/10.3208/sandf1972.15.3_1.

Esmaili, D., Hatami, K., and Miller, G.A., 2014, “Influence of Matric Suction on Geotextile Reinforcement-Marginal Soil Interface Strength.” *Geotextiles and Geomembranes* 42 (2): 139–53. https://doi.org/10.1016/j.geotexmem.2014.01.005.

Federal Highway Administration, 2009, “Mechanically Stabilized Earth Walls and Reinforced Soil Slopes.”, *Design and Construction Guidelines*., Publication No. FHWA-NHI- 10-025 , Washington DC

Hatami, K., and Boutin, J., 2022. “Influence of Backfill Type on the Load-Bearing Performance of GRS Bridge Abutments.” *Geosynthetics International* 29 (5): 506–519. https://doi.org/10.1680/jgein.21.00052.

Hatami, K., and Doger, R., 2021. “Load-Bearing Performance of Model GRS Bridge Abutments with Different Facing and Reinforcement Spacing Configurations.” *Geotextiles and Geomembranes* 49 (5): 1139–1048. https://doi.org/10.1016/j.geotexmem.2021.03.008.

Hatami, K., Miller, G.A., and Garcia L., 2010a, “Use of MSE Technology to Stabilize Highway Embankments and Slopes in Oklahoma”, *Oklahoma Department of Transportation, Tulsa, OK, USA, Final Report OTC REOS7-1-19*.

Hatami K., Garcia L.M. and Miller, G.A., 2010b, “Influence of moisture content on the pullout capacity of geotextile reinforcement in marginal soils”, *61st Highway Geology Symposium, Oklahoma City, OK*.

Hatami, K., Miller, G.A., and Granados, J.E., 2012, “Influence of Backfill Moisture Content on the Pullout Capacity of Geotextile Reinforcement in MSE Walls.” OTCREOS10.1-18-F. https://rosap.ntl.bts.gov/view/dot/27059.

Jia, Y., Xu, C., Zhang, J., Zheng, J.J., and Zheng, Y., 2024. “Evaluation of Dynamic Soil Stress Distribution in GRS Bridge Abutments Subjected to Cyclic Loading.” *Geotextiles and Geomembranes* 52 (4): 855–69. https://doi.org/10.1016/j.geotexmem.2024.05.003.

Kilic, I. E., Cengiz, C., Edincliler, A., and Guler, E., 2021, “Seismic Behavior of Geosynthetic-Reinforced Retaining Walls Backfilled with Cohesive Soil.” *Geotextiles and Geomembranes* 49 (5): 1256–69. https://doi.org/10.1016/j.geotexmem.2021.04.004.

Kumar, A., Ohri, M. L., and Bansal, R. K., 2007, “Bearing Capacity Tests of Strip Footings on Reinforced Layered Soil.” *Geotechnical and Geological Engineering* 25 (2): 139–150. https://doi.org/10.1007/s10706-006-0011-6.

Mirzaalimohammadi, A., Ghazavi, M., Roustaei, M., and Lajevardi, S.H., 2019, “Pullout Response of Strengthened Geosynthetic Interacting with Fine Sand.” *Geotextiles and Geomembranes* 47 (4): 530–41. https://doi.org/10.1016/j.geotexmem.2019.02.006.

Mirzaeifar, H., Hatami, K., and Abdi, M.R., 2022, “Pullout Testing and Particle Image Velocimetry (PIV) Analysis of Geogrid Reinforcement Embedded in Granular Drainage Layers.” *Geotextiles and Geomembranes* 50: 1083–1109. https://doi.org/10.1016/j.geotexmem.2022.06.008.

National Concrete Masonry Association, 2006, “*Design Manual for Segmental Retaining Walls*”, 3rd Edition.

National Cooperative Highway Research Program, 2009, " Selecting Backfill Materials for MSE Retaining Walls", *Transportation Research Board.*, https://onlinepubs.trb.org/onlinepubs/nchrp/docs/NCHRP24-22_FR.pdf

Riccio, M., Ehrlich, M., and Dias, D., 2014, "Field Monitoring and Analyses of the Response of a Block-Faced Geogrid Wall Using Fine-Grained Tropical Soils." *Geotextiles and Geomembranes* 42 (2): 127–138. https://doi.org/10.1016/j.geotexmem.2014.01.006.

Sandri, D., 2005, "Drainage Recommendations for MSE Walls Constructed with Marginal Fills." In *Proceedings of North American Geo-synthetics Conference (NAGS2005), Las Vegas, Nevada, USA, GRI-19 (CD-volume).*

Shivashankar, R., and Jayaraj, J., 2014, "Behaviour of Prestressed Geosynthetic Reinforced Granular Beds Overlying Weak Soil." *Indian Geotechnical Journal* 44 (1): 26–38. https://doi.org/10.1007/s40098-013-0070-6.

Tatsuoka, F., Hirakawa, D. , Nojiri, M., Aizawa, H., Tateyama, M., and Watanabe, K., 2007. "A New Type Integral Bridge Comprising of Geosynthetic-Reinforced Soil Walls." In *New Horizons in Earth Reinforcement*. CRC Press.

Vahedifard, F., Tehrani, F.S., Galavi, V., Ragno, E., and AghaKouchak, A., 2017, "Resilience of MSE Walls with Marginal Backfill under a Changing Climate: Quantitative Assessment for Extreme Precipitation Events." *Journal of Geotechnical and Geoenvironmental Engineering* 143 (9): 04017056. https://doi.org/10.1061/(ASCE)GT.1943-5606.0001743.

Xu, P., Li, T., and Hatami, K., 2020. "Limit Analysis of Bearing Capacity and Failure Geometry of GRS Bridge Abutments." *Computers and Geotechnics* 127 (November):103758. https://doi.org/10.1016/j.compgeo.2020.103758.

Yang, K., Wu, H., Tseng, T., and Yoo, C., 2023, "Model Tests of Geosynthetic-Reinforced Soil Walls with Marginal Backfill Subjected to Rainfall." *Geotextiles and Geomembranes* 51 (2): 342–359. https://doi.org/10.1016/j.geotexmem.2022.12.002.

Yoo, C., 2013, "Effect of Rainfall on Performance of Geosynthetic Reinforced Soil Wall Using Stress-Pore Pressure Coupled Analysis." In *Geo-Congress 2013*, 566–573. San Diego, California, United States: American Society of Civil Engineers. https://doi.org/10.1061/9780784412787.059.

Yoo, H., Kim, H., and Jeon, H., 2007, "Evaluation of Pullout and Drainage Properties of Geosynthetic Reinforcements in Weathered Granite Backfill Soils." *Fibers and Polymers* 8 (6): 635–641. https://doi.org/10.1007/BF02876002.